c-axis electrical transport at the metamagnetic transition in the heavy-fermion superconductor UTe_2 under pressure

G. Knebel,[1,*] A. Pourret,[1] S. Rousseau,[1] N. Marquardt,[1] D. Braithwaite,[1] F. Honda,[2,3] D. Aoki,[1,2] G. Lapertot,[1] W. Knafo,[4] G. Seyfarth,[5] J-P. Brison,[1] and J. Flouquet[1]

[1]*Université Grenoble Alpes, CEA, Grenoble INP, IRIG, PHELIQS, F-38000 Grenoble, France*

[2]*Institute for Materials Research, Tohoku University, Oarai, Ibaraki, 311-1313, Japan*

[3]*Central Institute of Radioisotope Science and Safety, Kyushu University, Fukuoka 819-0395, Japan*

[4]*Laboratoire National des Champs Magnétiques Intenses–EMFL, CNRS, Université Grenoble Alpes, INSA-T, Université Toulouse 3, F-31400 Toulouse, France*

[5]*Laboratoire National des Champs Magnétiques Intenses (LNCMI), CNRS, Université Grenoble Alpes, F-38042 Grenoble, France*

(Received 23 June 2023; revised 28 February 2024; accepted 29 February 2024; published 1 April 2024)

The electrical resistivity of the unconventional superconductor UTe_2 shows very anisotropic behavior in the normal state depending on the current direction. In this paper we show that the maximum in the resistivity ρ_c for current applied along the c axis at $T_{\rho_c}^{\max} \approx 14.75$ K follows the minimum in the thermal expansion $T_\alpha^\star$ along the b axis. Under a magnetic field applied along the b axis, $T_{\rho_c}^{\max}$ can be tracked up to the critical point of the first-order metamagnetic transition, which is located near 6 K and 34.5 T. Surprisingly, at the metamagnetic field H_m the resistivity ρ_c shows a steplike decrease while the resistivities ρ_a and ρ_b, for current along the a and b axes, respectively, show a steplike increase. Under hydrostatic pressure $T_{\rho_c}^{\max}$ and H_m decrease significantly up to the critical pressure p_c at which superconductivity is suppressed and a long-range antiferromagnetic order appears. We show that the phase diagram at different pressures can be scaled by $T_{\rho_c}^{\max}$ in field and temperature, suggesting that this temperature scale is governing the main interactions in the normal state.

DOI: 10.1103/PhysRevB.109.155103

I. INTRODUCTION

The discovery of superconductivity in UTe_2 has raised an intense research effort due to the possible spin-triplet pairing [1–3]. Indication for this rare pairing state is the strong enhancement of the superconducting upper critical field H_{c2}, which exceeds by far the Pauli limit of superconductivity for all three crystallographic axes. Another one is the change of this paramagnetic limit in the different superconducting phases observed under pressure for field along the easy a axis [4]. Knight shift measurements in magnetic resonance experiments (NMR) suggest a possible spin-triplet superconducting state too [5–7]. Moreover, a quite singular property of superconductivity in UTe_2 is that the pairing strength itself is sensitive to the magnetic field for all crystal axes [8]. For a field applied along the b axis, superconductivity is enhanced above $H^\star \approx 17$ T [9,10], and a phase transition between two superconducting phases, the low-field superconducting phase (lfSC) and a high-field phase (hfSC), have been evidenced by specific heat [8], and independently by combined NMR and ac susceptibility measurements [11]. This shows that the field-induced hfSC is a bulk superconducting phase. It is limited by a metamagnetic transition at $\mu_0 H_m \approx 35$ T [9,10]. The first-order metamagnetic transition is characterized by a large jump of the magnetization [12], a volume discontinuity [13], and a jump in the magnetoresistance with the current applied along the a axis [14]. It is accompanied by a strong increase of the Sommerfeld coefficient γ of the specific heat [8,15,16] and of the A coefficent of the Fermi-liquid resistivity [14,17]. Recent NMR measurements show that critical longitudinal magnetic fluctuations start to develop for $H > H^\star$ and are diverging in the vicinity of H_m [18]. An abrupt Fermi-surface change at H_m has been discussed from Hall effect measurements [19], but constitutes still an open question [20]. Superconductivity in UTe_2 was claimed to be topologically nontrivial following the detection of chiral-edge states in scanning-tunneling microscopy (STM) [21], and of broken time-reversal symmetry in Kerr effect studies [22]. However, these results are still discussed controversially and may depend on the sample quality [23,24].

Under hydrostatic pressure, two superconducting phases occur above 0.3 GPa, indicating multiphase superconductivity at zero field [25–27]. Different superconducting phases have been confirmed by measurements under magnetic field applied along the a and b axes at constant pressure [27,28]. The superconducting phases are suppressed at a critical pressure $p_c \approx 1.5$–1.7 GPa (depending on the pressure medium) and a magnetically ordered state occurs. Initially a ferromagnetic state has been expected [29], but recent neutron diffraction experiments confirm an incommensurate antiferromagnetic order above p_c [30]. The magnetic anisotropy is reversed at p_c [31–34]. While the a axis is the easy magnetization axis at ambient pressure, it switches to the b axis in the pressure-induced magnetic phase. The change in the magnetic anisotropy has also a feedback on the superconducting state under pressure.

*georg.knebel@cea.fr

Close to p_c, the upper critical field H_{c2} is the highest for the c axis, and even reentrant superconductivity occurs in this direction [4,29,33,35].

To understand the occurrence of these various superconducting phases in UTe_2 the knowledge of the electronic structure and of the magnetic fluctuations is necessary. Various electronic band structure calculations indicate cylindrical Fermi surfaces along the c axis [36–41]. Experimentally, the Fermi surface of UTe_2 is not fully determined, but angle-resolved photoemission spectroscopy (ARPES) experiments [39] and quantum oscillations have confirmed the quasi-two-dimensional Fermi-surface sheets [42–45].

Resistivity measurements with different current directions suggest that UTe_2 is a three-dimensional metal [46], indicating that either the cylinders are strongly corrugated or that a three-dimensional Fermi surface is missing in quantum oscillation experiments. For currents applied along the a and b axes, the temperature dependence of the resistivity shows a broad maximum near 60 K and drops for lower temperatures, indicating the formation of coherent quasiparticle bands characteristic of a heavy-fermion state. Once a nonmagnetic background of the scattering is subtracted, this maximum is shifted down to the temperature scale $T_{\chi_b}^{\max} \approx 35$ K, for which the susceptibility and the Hall effect for $H \parallel b$ are maximum [17,19,33]. For a current applied along the c axis a distinct maximum of the resistivity appears only at $T_{\rho_c}^{\max} \approx 14.5$ K [17,46–48]. Near this characteristic temperature several other quantities show anomalies: the electronic specific heat has a broad maximum [49], the thermal expansion coefficients along the c and b axes have a minimum [26,49], the thermoelectric power has a minimum [50], and the a axis susceptibility χ_a as well as the Knight shift becomes constant at lower temperatures [51]. The anomaly at $T^\star$ corresponds to the crossover to a coherent low-temperature regime [46,52]. Furthermore, inelastic neutron scattering experiments show the development of a magnetic excitation below $T \approx 60$ K at the incommensurate wave vector $\mathbf{k_1} = (0, 0.57, 0)$ which is maximal at the energy transfer 3–4 meV [52–54]. They also reveal that these fluctuations are low dimensional and antiferromagnetic, saturating below $T^\star \approx 15$ K [53,54]. They become gapped in the superconducting state [55,56].

In this paper, we study the field and pressure dependence of the different fluctuations by electrical resistivity measurements. The paper is divided in different sections. In Sec. II we will present the experimental details and give a summary of all samples studied in this work. Section III presents ambient pressure results: we will show the field dependence ($H \parallel b$) of the $T^\star$ anomaly in the resistivity with current applied along the c axis (ρ_c) and longitudinal thermal expansion measurements (α_b) up to the metamagnetic field. We will demonstrate that the maximum ρ_c at $T^\star$ can be followed up to the metamagnetic transition. Further, we will discuss the anisotropy of the magnetoresistivity for currents applied along the a, b, and c axes. Finally, we will compare the superconducting phase diagram in a field $H \parallel b$ for different samples with different T_{SC}. We find that the lfSC phase scales with T_{SC}, while the hfSC is strongly affected by sample quality.

In the following Sec. IV we will concentrate on the resistivity measurements under high pressure. In Sec. IV A the temperature dependence of the resistivity under pressure for a current applied along the c axis is presented and compared to those with a current along the a axis. We present the pressure-temperature phase diagram of UTe_2 at zero magnetic fields. In Sec. IV B we present the temperature and field dependence of ρ_c under pressure. In Sec. IV C we discuss the obtained magnetic field-temperature phase diagrams for the different pressures. We show that the phase diagrams for the different pressures scale with the temperature $T^\star$, indicating the importance of the fluctuations connected with this energy scale. Magnetoresistivity gives evidence that the order, which occurs above the critical pressure, is antiferromagnetic in agreement with recent neutron diffraction results [30]. Finally, in Sec. V we give a short conclusion. Additional data supporting the analyses are presented in the Appendix.

TABLE I. Summary of single crystals used in this study and the corresponding measurements.

	Crystal growth	T_{SC} (K)	Measurement
S1a	CVT	1.84	$\rho_c(T,H), J \parallel\sim c, p = 0$ (current not perfectly aligned)
S1b	CVT	1.85	$\rho_c(T,H), J \parallel c, p \neq 0$
S2	CVT	1.45	α_b, same crystal as in [8]
S3	MSF	2.0	$\rho_a(H), J \parallel a, p = 0$
S4	CVT	1.82	$\rho_b(H), J \parallel b, p = 0$
S5	CVT	1.85	$\rho_c(H), J \parallel c, p = 0$ (not perfectly aligned in field)

II. EXPERIMENTAL METHODS

In this study single crystals of UTe_2 grown by chemical vapor transport (CVT) using iodine as transport agent [57] and by the molten salt flux (MSF) method [58] have been investigated. An overview of all samples is given in Table I. At ambient pressure we studied the dependence of the current direction on the electrical resistivity and on the A coefficient of the Fermi-liquid resistivity. For $J \parallel b$ (sample S4) and $J \parallel c$ (samples S1a, S5) single crystals grown by CVT have been investigated with superconducting transitions $T_{SC} \approx 1.85$ K at zero field (throughout the paper, the superconducting transition temperature T_{SC} in the resistivity is defined by the criteria $\rho = 0$, see Fig. 1). CVT grown samples have been cut from large crystals with a spark cutter after alignment using a Laue photograph. Typical dimensions of these CVT crystals are $1 \times 0.3 \times 0.15\text{mm}^3$. Two different crystals have been used for measurements with current $J \parallel c$. For sample S1a, the alignment of the contacts has probably not been perfectly done due to its irregular, non barelike shape, and the absolute value of the resistivity of this sample is smaller than expected from literature [46,47]. We studied in addition a second sample S5 ($0.8 \times 0.15 \times 0.1\text{mm}^3$) which has a similarly high resistance; unfortunately, here the field orientation is not perfect as the measured metamagnetic transition in this experiment is higher than expected (data are shown in the Appendix Fig. 21). For resistivity measurements with current $J \parallel a$ axis (ρ_a) we used a MSF sample with a $T_{SC} \approx 2$ K. The MSF sample had a naturally needlelike shape along the a axis with dimensions of $2 \times 0.2 \times 0.2\text{mm}^3$. The high-pressure resistivity experiments with current along c have been performed on a bare-shape-like

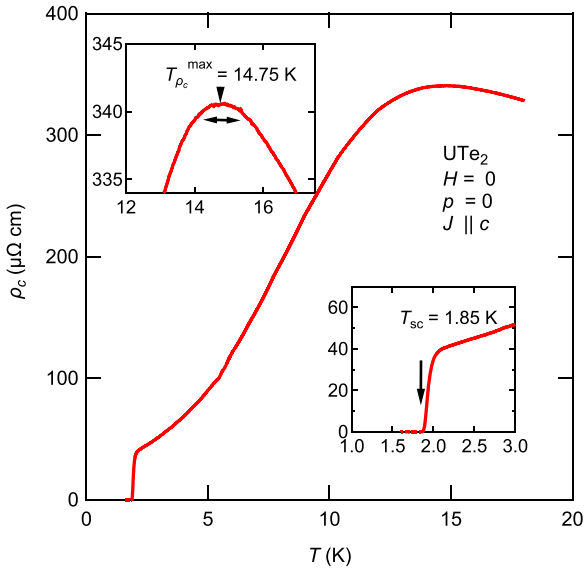

FIG. 1. Example for the definition of the superconducting transition temperature T_{SC} and the maximum $T^\star$ from the resistivity data at $p = 0$ and $H = 0$. In the phase diagrams in the following the error bars for T_{SC} is in all cases smaller than the symbol size and thus we do not plot error bars. We note that the discussion of the transition width from resistivity data alone is difficult as it is not a bulk probe. The upper inset shows a zoom on the anomaly at $T^\star$, the horizontal arrow shows the maximal error of the determination.

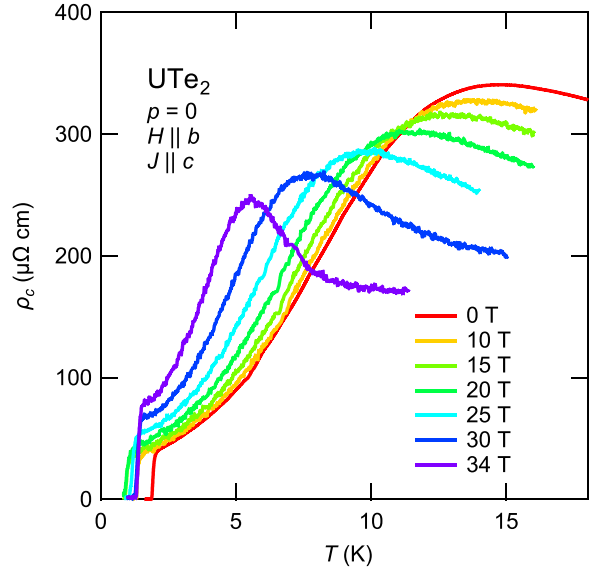

FIG. 2. Temperature dependence of the electrical resistivity $\rho_c(T)$ of UTe$_2$ with current $J \parallel c$ at different magnetic fields $H \parallel b$ (measured on sample S1a). The maximum of the resistivity $T_{\rho_c}^{max}$ shifts with field from $T_{\rho_c}^{max} = 14.75$ K at $H = 0$ to 5.5 K at 34 T.

sample (S1b) which is cut from the same single crystal as S1a with current applied along the c axis. For the measurements with current along a we refer to our previous results reported partly in Ref. [4].

Electrical resistivity measurements have been performed with a standard four-point lock-in technique with a maximal applied current of 0.5 mA for the measurements at ambient pressure and 1 mA in the high-pressure cell. For all samples, electrical contacts to the samples have been performed by spot welding 15-μm-diameter Au wires on a freshly polished surface of the crystal as it is known that the surface of UTe$_2$ is very sensitive to air. To strengthen the electrical contacts mechanically, tiny drops of conducting silver paste have been added on top of the welded contacts. The contact resistance is typically of the order of several mΩ, but this has not been further studied.

The high-field transport measurements have been performed at the high magnetic field laboratory LNCMI in Grenoble using the resistive 36-T magnet M9 using a ^{3}He cryostat with a base temperature near 400 mK. We used a MP35N piston cylinder pressure cell to apply pressures up to 1.61 GPa with Daphne 7373 oil as pressure medium for the high-pressure resistivity experiment. The outer diameter of the pressure cell is only 15 mm which fits very close to the inner diameter of the vacuum can of the cryostat (16 mm). The high-pressure experiments have been performed up to a maximal field of 35 T. The temperature has been measured with a calibrated RuO$_2$ chip which is glued on the pressure cell. The lowest temperature in the pressure cell was $T_{min} \approx 1.2$ K.

Thermal expansion measurements at zero pressure have been performed using a high-resolution capacitive dilatometer [59] in the LNCMI Grenoble on the magnet M10 with a maximal field of 30 T in the temperature range from 2 to 25 K. The CVT grown sample (S2) with $T_{SC} \approx 1.5$ K was already studied in Ref. [8] by magnetostriction experiments.

III. AMBIENT PRESSURE RESULTS

A. c-axis transport and field dependence of $T^\star$

Figure 2 displays the temperature dependence of the c-axis resistivity ρ_c for different magnetic fields applied along the b axis below 20 K. A maximum of the resistivity at $T_{\rho_c}^{max} \approx 14.75$ K occurs at $H = 0$, similar to ρ_c measurements [17,46]. However, as already mentioned above, the absolute value of the resistivity ρ_c at low temperature is smaller than in previous reports [17,46,47], which might be due to a nonperfect alignment of the current with respect to the c axis. Under magnetic field $T_{\rho_c}^{max}$ shifts to a lower temperature and the maximum gets more pronounced. At the highest field of 34 T, just below the metamagnetic transition, $T_{\rho_c}^{max} \approx 5.5$ K. It is close to the critical point of the first-order metamagnetic transition which is located near 6 K and 34.5 T. Superconductivity, defined by $\rho = 0$, occurs in zero field below $T_{SC} = 1.85$ K. The minimum of T_{SC} ($T_{SC} = 0.88$ K) is found at $H^\star \approx 18$ T. For higher fields the temperature of zero resistivity increases again and at 34 T, $T_{SC} = 1.35$ K. This behavior of $H_{c2}(T)$ is similar to that of previous reports [9,10,60]. The highest T_{SC} of the hfSC phase is found just below H_m.

In the normal state above T_{SC} the resistivity ρ_c follows a Fermi-liquid temperature dependence $\rho(T) = \rho_0 + AT^2$, where ρ_0 is the residual resistivity and A the coefficient of the electron-electron scattering term. This is shown in Fig. 3, which shows ρ_c as a function of T^2 for several magnetic fields [61]. While at 10 T the fitting range is up to about 6 K, for the highest field this range is strongly reduced and the maximum temperature of the fit is about 4 K, i.e., the fitting range of the T^2 dependence is small so that the following analysis of the

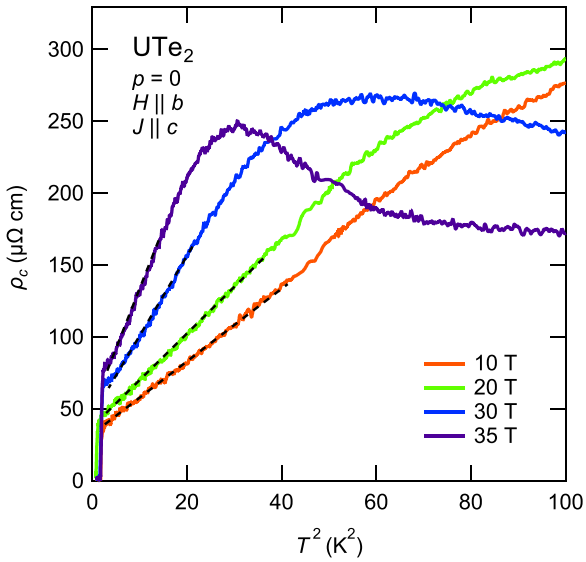

FIG. 3. (a) Temperature dependence of the resistivity ρ_c as a function of T^2 for different magnetic fields up to 34 T. The dashed lines present a fit with $\rho_c = \rho_0 + AT^2$. The range of the T^2 regime decreases with increasing magnetic field. Close to the metamagnetic field a fit with a free exponent n [Fig. 21(a)] would result in an exponent $n = 3$, but in the analysis of the Fermi-liquid A coefficient, we fixed the exponent to be $n = 2$.

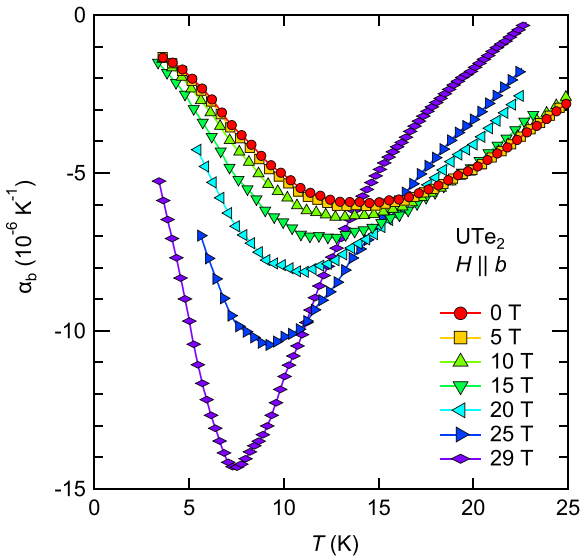

FIG. 4. Longitudinal thermal expansion α_b as a function of temperature for different magnetic fields applied along the b axis up to 29 T. $\alpha_b(T)$ shows a pronounced minimum, which we refer as $T_\alpha^\star$ in the text. Measurements are performed on sample S2.

A coefficient is rather qualitative. Anyway, in heavy-fermion systems the relation $A \propto \gamma^2$ is often obeyed indicating that local fluctuations dominate [62]. In a simplified picture, the A coefficient is an indirect measure the square of the effective mass $m^\star$ of the charge carriers. One has to keep in mind that resistivity in difference to specific heat is a directional probe and so in addition to the scattering time it depends also on the topology of the Fermi surface and not only on the density of states. The field dependence of A and the residual resistivity ρ_0 will be discussed below.

Figure 4 shows the longitudinal thermal expansion coefficient along the b axis α_b as a function of temperature at different magnetic fields. $\alpha_b(T)$ is negative and has a very broad minimum at $T_\alpha^\star \approx 14.5$ K in zero field. A magnetic field applied along the b axis shifts $T_\alpha^\star$ to lower temperatures and the minimum sharpens significantly. We can follow the minimum up to the highest field of 29 T and $T_\alpha^\star(H)$ determined from thermal expansion is in excellent agreement with the maximum $T_{\rho_c}^{\max}$ in the c-axis transport. Figure 5 shows the phase diagram of UTe_2 at ambient pressure determined from the c-axis transport and the thermal expansion along the b axis. This shows that the thermodynamic anomaly detected at $T_\alpha^\star$ connects to the metamagnetic transition at H_m. The $T_\alpha^\star \approx T_{\rho_c}^{\max}$ is a signature of a crossover to the low-temperature state. In heavy-fermion compounds this crossover arises from the interplay of the onsite and intersite magnetic interactions, which result in the formation of the coherent heavy-fermion state on cooling. In UTe_2 this crossover is also visible in the evolution of the magnetic fluctuations at finite wave vectors [46,51–54]. In addition to the magnetic fluctuations, crystal-field effects may also play a role in the microscopic origin of the $T^\star$ anomaly [63].

B. Anisotropic transport at H_m

Previous magnetoresistivity measurements with a current $J \parallel a$ axis showed that $\rho_a(H)$ in the normal state just above T_{SC} increases abruptly at the metamagnetic transition H_m by a factor of 4 [14,19,64]. A hysteresis between field up and down sweeps of about 0.2 T indicates the first-order nature of the

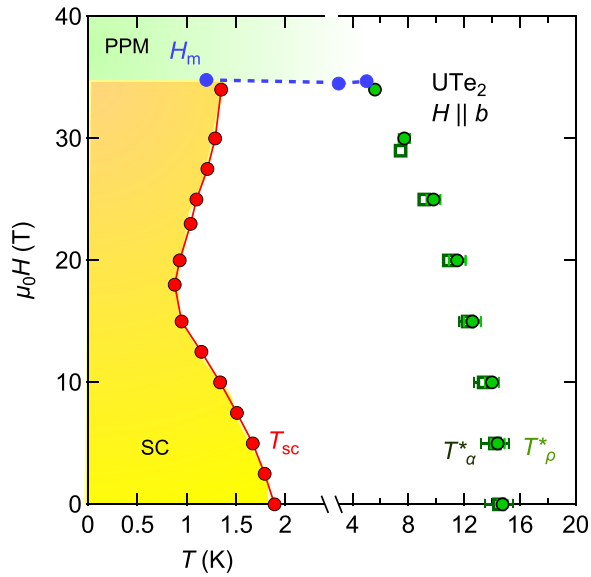

FIG. 5. Phase diagram of UTe_2 for field along the b axis from the c-axis transport and the thermal expansion measurements. T_{SC} is the superconducting transition temperature, $T_\alpha^\star$ the minimum in the thermal expansion coefficient α_b, $T_{\rho_c}^{\max}$ the maximum in $\rho_c(T)$, and H_m the field of the metamagnetic transition. Clearly, the maximum $T_{\rho_c}^{\max}$ coincides with the temperature of the minimum in the thermal expansion. T_{SC} is determined by the criterion $\rho = 0$ and error bars are smaller than the symbol size.

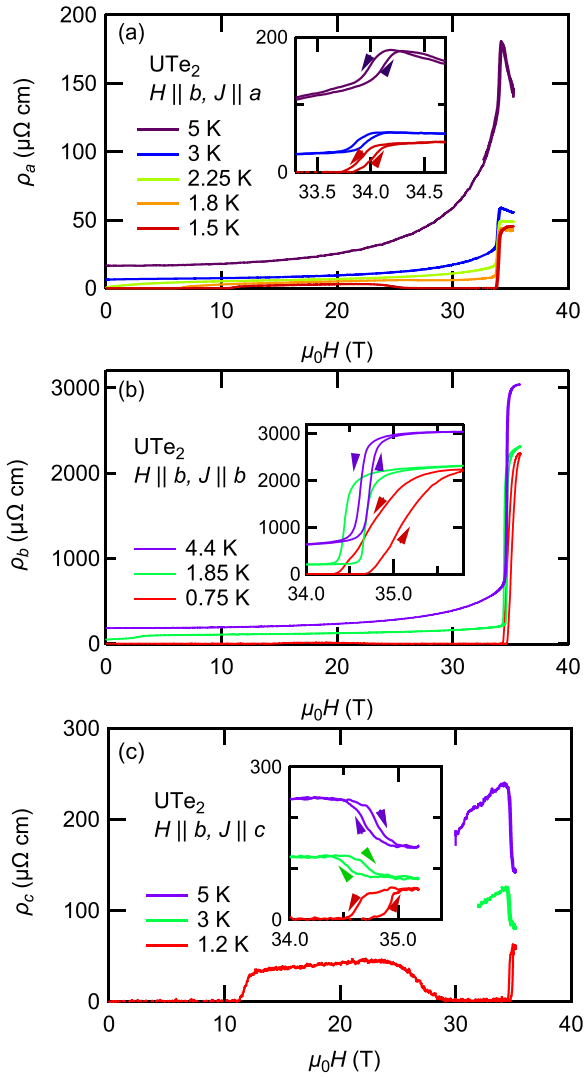

FIG. 6. Magnetoresistivity for $H \parallel b$ at different temperature with the current applied along a, b and c axes. The inset in every panel gives the field range of the metamagnetic transition in an enlarged scale. [MSF grown sample S3 for $J||a$, CVT grown samples for $J||b$ (S4) and $J||c$ (S1a).]

transition. The transition is sharp up to a critical point of $\approx$6 K where the the hysteresis vanishes. At higher temperatures a broad crossover from a coherent correlated paramagnetic to an incoherent paramagnetic state occurs. A similar abrupt change in the Hall resistivity as a function of field at H_m together with a change of the main charge carriers observed in thermoelectric power experiments [19] suggest that an abrupt change of the Fermi surface occurs at the metamagnetic transition H_m. Figure 6 displays the magnetoresistivity with a current injection along the a, b, and c axes as a function of the magnetic field applied along the b axis. For the $J \parallel a$ axis, we used a high-quality MSF grown sample with a $T_{SC} = 2$ K. $\rho_a(H)$ of the MSF sample with the higher T_{SC} shows a similar field dependence in the normal state as reported previously [14,64]. The samples used for the different current directions show re-entrant superconductivity at the lowest temperature up to H_m.

For a current $J \parallel b$ axis, ρ_b shows an extremely large positive jump at H_m, by a factor 8.5 at 2.25 K in the normal state [see Fig. 6(b)]. This jump is much stronger than that being observed for a current applied along the a axis.

Astonishingly, for a current $J \parallel c$ axis, the magnetoresistivity $\rho_c(H)$ drops at the metamagnetic transition as shown in the lower panel of Fig. 6(c); at 3 K the magnetoresistivity decreases by a factor of 1.45, i.e. the change of the magnetoresistivity at the metamagnetic transition is much smaller and opposite to that observed along the a and b directions, and for T near T_{SC} no strong anomaly occurs near H_m. With increasing temperatures above T_{SC} the drop of the resistivity along c becomes stronger and changes into a crossover above the critical point of the metamagnetic transition line, like for the other current directions (see also Ref. [17]). These distinct differences between the magnetoresistivity measured for the different current directions might be due to the anisotropic quasi-two-dimensional (quasi-2D) Fermi surface of UTe_2 [42–44], but a detailed microscopic picture of the anisotropic scattering is still missing. In Ref. [46], within a simple two-band model, it has been proposed that the conduction along the c axis is dominated by a heavy Z pocket of the Fermi surface detected in ARPES measurements, while the conduction along the a- and b-axis directions is dominated mainly by the cylindrical Fermi surfaces. Recent de Haas–van Alphen (dHvA) quantum oscillation experiments did not detect such a small three-dimensional (3D) Fermi-surface pocket [42,43,45] in difference to Ref. [44] where a 3D Fermi-surface pocket may be observed using a tunnel diode oscillator circuit (TDO); future experimental investigations have to clarify this point.

An anisotropy of the transport properties at a metamagnetic transition has been also observed in other heavy-fermion compounds. In the paramagnetic and nearly antiferromagnetic $CeRu_2Si_2$, where the metamagnetic transition occurs for a field applied along the easy c axis, the magnetoresitivity shows a positive jump in the transverse configuration $J \parallel a$, while a peak occurs for $J \parallel c$ [65]. In the paramagnetic and nearly ferromagnetic UCoAl the magnetoresistance has a positive jump at $\mu_0 H_m \approx 0.6$ T for $J \parallel H \parallel c$, which is the easy magnetization axis, but a negative jump occurs in the transverse configuration [66]. And in antiferromagnetic UPd_2Al_3, a sharp peak occurs at H_m in the longitudinal configuration while a strong decrease of almost 50% occurs in the transverse magnetoresistance [67]. In all of these examples, the metamagnetic transition is accompanied by a Fermi-surface reconstruction [68–70], as proposed for UTe_2.

The field dependencies of the normalized A coefficient and of the residual resistivity ρ_0 extracted from Fermi-liquid fits are shown in Fig. 7 as a function of H/H_m. A and ρ_0 were determined from the temperature-dependent measurements (open circles for $J \parallel c$) and from the field sweeps at constant temperature (full symbols) (see also Figs. 21 and 22 in the Appendix). We compare $A(H)$ normalized to its zerofield value for the different current directions in Fig. 7 (see also in the Appendix Fig. 23 which shows the absolute values). The anisotropy of the A coefficient at zero field is similar to that in Ref. [46]. The field dependence of A for $J \parallel a$ determined on the new MCF sample is in excellent agreement with those

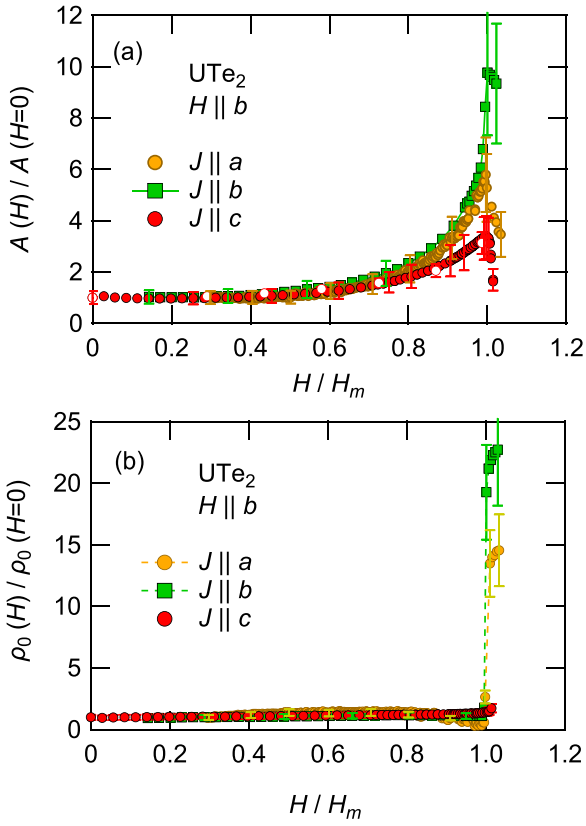

FIG. 7. Normalized A coefficient determined from a Fermi-liquid temperature dependence $\rho(T) = \rho_0 + AT^2$ of the resistivity for current applied along the a, b, and c directions as a function of H/H_m. Full symbols are determined from the measured field sweeps at different temperatures. Fits have been performed for $T < 3.5$ K $J \parallel a$ (sample S3), $T < 4.5$ K for $J \parallel b$ (S4), and $T < 4$ K for $J \parallel c$ (S5, data shown in Fig 21). Open symbols for $J \parallel c$ are from fits of data shown in Fig. 2 (sample S1a). The lower panel (b) shows the residual resistivity ρ_0 obtained from the Fermi-liquid fit for the three current directions.

published in Ref. [14]. However, there are distinct differences in the field dependence of $A(H)$ for the different directions.

For $J \parallel a$ axis the absolute value of A is the smallest and it increases from about $A = 0.6$ μΩ cm K^{-2} at zero field to 4 μΩ cm K^{-2} at H_m. Astonishingly, the field enhancement of A is symmetric around H_m, which was not expected owing to the first-order character of the metamagnetic transition. For current along the b axis, the absolute value of A equals 5 μΩ cm K^{-2} at zero field. $A(H)$ increases very strongly by a factor of 10, when the metamagnetic transition is approached. [The absolute value of $A(H)$ for the b-axis direction may be overestimated as it is only determined from the measured field dependencies at different temperatures, and no temperature-dependent measurements at fixed field have been performed (shown in the Appendix)].

In zero field, the value of A is the highest for a current applied along the c axis, with $A = 8.3$ μΩ cm K^{-2}. On approaching the metamagnetic transition under magnetic field, A increases only by a factor of 3.4 at H_m for $J \parallel c$ and decreases abruptly just above the metamagnetic transition. If we compare the value at zero field with Sommerfeld coefficient

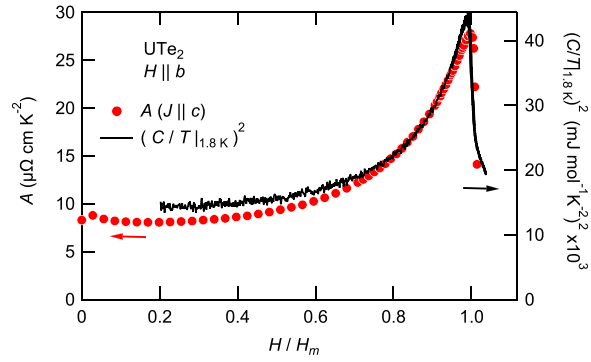

FIG. 8. Field dependence of the A coefficient determined from the resistivity measurements with $J \parallel c$ and $(C/T)^2$ measured at 1.8 K as a function of magnetic field normalized to the metamagnetic transition field H_m. Both quantities scale surprisingly well. Especially the very sharp drop at the metamagnetic transition is only observed in the measurement of the A coefficient with current applied along the c axis, while for current in the other directions, the enhancement of the Fermi-liquid A coefficient occurs to be more symmetric around H_m.

at zero field of 120 mJ mol^{-1} K^{-2} we find that A/γ^2 is much higher than the standard value of the Kadowaki-Woods ratio of 1×10^{-5} μΩ cm(K mol/mJ)^2, commonly expected in a Kondo lattice. The main reason for this strong difference is the quasi-2D Fermi surface in UTe_2 and, thus, leading to a strongly anisotropic A coefficient. By contrast, if we compare the field dependence of the square of the specific heat divided by temperature C/T at 1.8 K and that of the A coefficient determined from ρ_c (see Fig. 8), we find an excellent agreement of both properties. Especially, the strong drop of the $C/T|_{T=1.8\,\mathrm{K}}$ does not occur in the $A(H)$ for the other directions.

Figure 7(b) shows the field dependence of the residual resistivity ρ_0 normalized to its value in zero field. We clearly see that ρ_0 for the a and b axes increases by a factor of at least 15 (a) or 20 (b), while the change of ρ_0 along c is very small. The strong increase of the residual resistivity for $J \parallel a$ and b cannot be only due to a change in the charge carrier density, as this should influence the change of the magnetoresistance for $J \parallel c$ at H_m in rather similar way. In a simple picture it may also be an indication for a Fermi-surface change at H_m as has been previously suggested from the thermoelectric response through H_m [19]. Surely, the change of the Fermi surface above H_m is still an open question.

C. Comparison of the superconducting phase diagrams

In Fig. 9(a) we compare the superconducting upper critical field H_{c2} with $H \parallel b$ for samples with different values of T_{SC} varying from 1.45 to 2 K. All samples show field-reentrant superconductivity in fields above $H^\star \approx 16$–18 T. The thermodynamic phase diagram has been only determined in one of the samples ($T_{SC} = 1.84$ K by specific-heat measurements [8]). The exact field of the reinforcement superconducting transition is difficult to determine from the transport experiments as it does not coincide exactly with the bulk transition [8,60]. As shown in Ref. [8], the anomaly in specific heat corresponding to the bulk transition to the hfSC

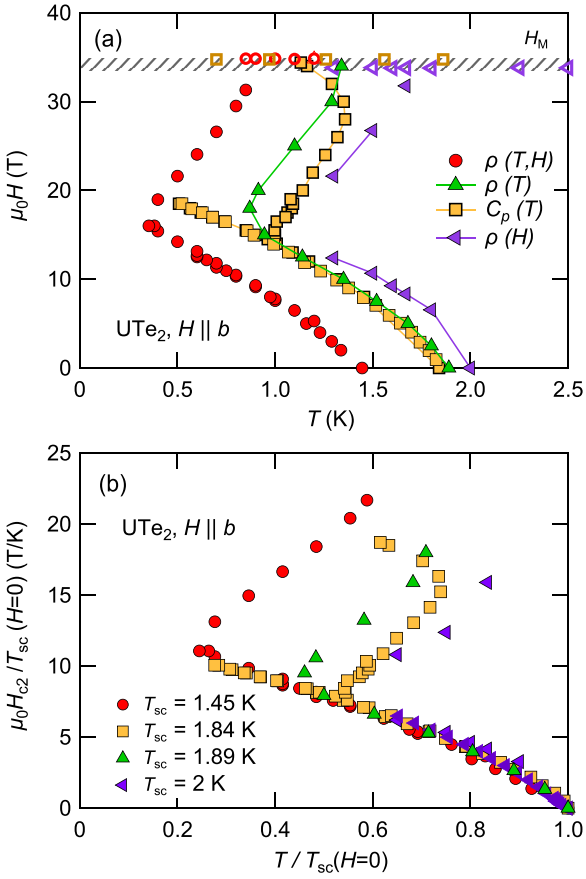

FIG. 9. (a) Comparison of the superconducting phase diagram of samples with different T_{SC} for field $H \parallel b$. [Red circles are taken from Ref. [9], yellow squares from specific-heat measurements of Ref. [8], green triangles up determined from data in Fig. 2, violet triangles from Fig. 5(a). The field of the metamagnetic transition is marked by open symbols, respectively. (b) Upper critical field normalized by T_{SC} versus T/T_{SC} for the different samples.

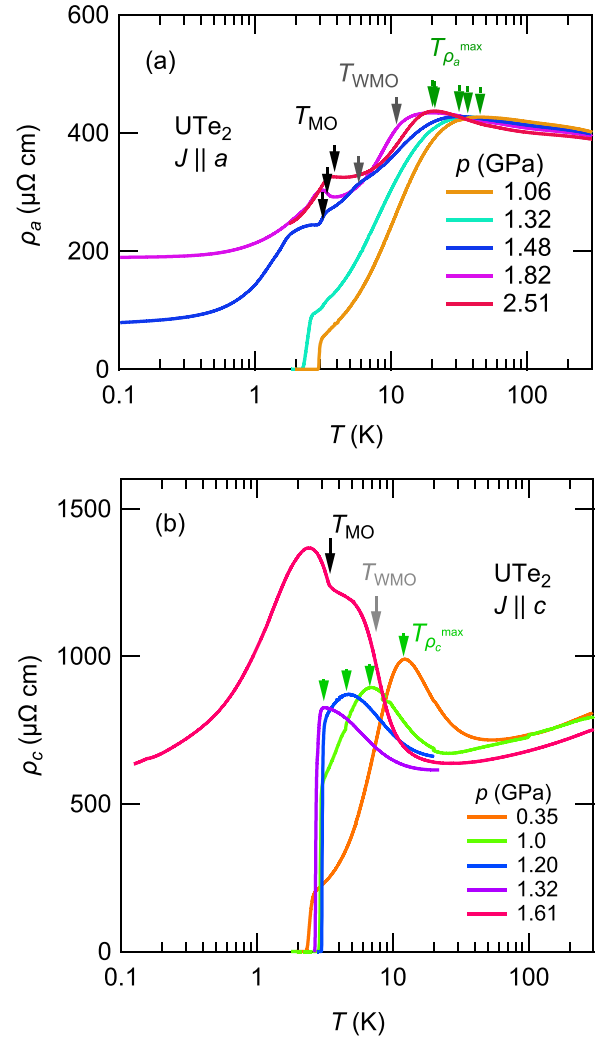

FIG. 10. Temperature dependence of the resistivity for (a) ρ_a (current $J||a$, data from the pressure experiment reported in Ref. [4]) in UTe$_2$ at different pressures on a logarithmic scale. The black and gray arrows indicate the ordering temperature T_{MO} and the crossover to a correlated regime T_{WMO}. (b) Temperature dependence of ρ_c (current $J||c$). The arrows indicate T_{MO}, T_{WMO}, and $T_{\rho_c}^{max}$.

phase appears as a hump and is extremely broad [71]. However, $H^\star$ is roughly independent of the sample quality [60]. We also see in Fig. 9(a) that the value of the measured metamagnetic field H_m varies from 33.8–34.75 T for the different samples. The lowest metamagnetic field has been found for the sample with the highest T_{SC}, while in samples with a lower T_{SC} a slightly higher H_m has been observed. The robustness of H_m for different sample qualities has also been reported in Ref. [72].

In Fig. 9(b) we plot H_{c2} normalized by T_{SC} as a function of T/T_{SC}. In this representation $H_{c2}(T/T_{SC})$ in the lfSC phase scales on a single curve for samples with different T_{SC}, while in the high-field phase hfSC the critical field strong variations occur depending on the samples. In general, in the clean limit, the orbital superconducting upper critical field at zero temperature depends on the Fermi velocities $v_{F_\perp}$ perpendicular to the applied magnetic field H and T_{SC} as $H_{c2}^{orb} \propto (\frac{T_{SC}}{v_{F_\perp}})^2$. However, in Fig. 9(b) we plot $\frac{\mu_0 H_{c2}}{T_{SC}}$ vs $\frac{T}{T_{SC}}$. This normalization is much better than that with a purely orbital limit $\frac{H_{c2}}{T_{SC}^2}$ vs $\frac{T}{T_{SC}}$ (see Fig. 24). As discussed in Ref. [8] the upper critical field for $H \parallel b$ is not described by a simple orbital limit. Surprisingly, as shown in Fig. 9, the lfSC and hfSC phases show very different behavior for the different samples. While the bulk nature of the hfSC phase has been clearly shown by specific heat, thermal expansion and ac susceptibility [8,11,60], the bulk transition itself is intrinsically very broad. The thermal expansion experiments clearly indicate different vortex dynamics in the lfSC and hfSC phases [8]. This is also supported by measurements of the critical current [73], indicating that pinning depends strongly on sample quality and impurities. Here, we observe that $H^\star$ [Fig. 9(a)], like H_m, appears weakly dependent on the sample purity [26,60] even though T_{SC} changes very significantly between samples.

IV. c-AXIS ELECTRICAL TRANSPORT UNDER PRESSURE

A. Comparison of c-axis and a-axis resistivity in zero field

Figure 10 displays the temperature dependence of the resistivity with a current along the a axis (ρ_a, upper panel) and

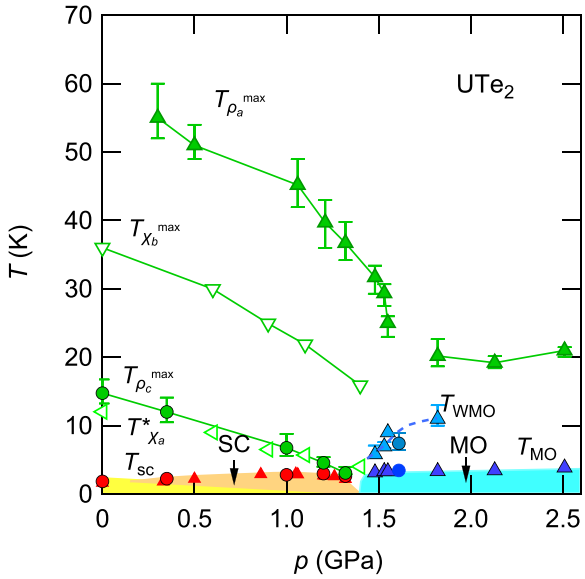

FIG. 11. Pressure-temperature phase diagram of UTe_2 at zero magnetic field indicating the pressure dependence of $T_{\rho_a}^{\max}$, $T_{\chi_b}^{\max}$ (taken from Ref. [4]), $T_{\rho_c}^{\max}$, $T_{\chi_a}^{\star}$ (taken from Ref. [31]), the superconducting transition temperature T_{SC} (red symbols, triangles taken from Ref. [4]), and the magnetic transition temperatures T_{MO} and T_{WMO}. (Triangles up and circles are from the a- and c-axis resistivity, respectively.)

along the c axis (ρ_c, lower panel) for different pressures at zero magnetic field. For both current directions, the general behavior at high temperature is similar to that at ambient pressure. $\rho_a(T)$ increases on cooling down to a temperature $T_{\rho_a}^{\max}$ and decreases to lower temperatures. The temperature of the broad maximum in ρ_a, $T_{\rho_a}^{\max}$, decreases with increasing pressure, and is minimum near the critical pressure $p_c \approx 1.5$ GPa. At p_c superconductivity is suppressed and the magnetically ordered ground state is formed (see Fig. 11). $T_{\rho_a}^{\max}$ increases slightly above p_c. The exact position of p_c depends on the pressure conditions; $p_c \sim 1.7$ GPa has been reported in Refs. [25,33] using anvil pressure cells.

The temperature dependence of ρ_a shows a kink for $p = 1.48$ GPa near the temperature $T_{WMO} \approx 6$ K and a second anomaly near $T_{MO} \approx 3.5$ K in agreement with the previous report of two magnetic anomalies above p_c [31,32,35]. While at T_{MO} long-range magnetic order appears, T_{WMO} has been identified in magnetization measurements under pressure as a crossover to a weakly magnetically ordered state [31]. With increasing pressure, T_{WMO} shifts to higher temperature, gets less pronounced, and cannot be resolved anymore above 2 GPa as it gets close to $T_{\rho_a}^{\max}$. The lower anomaly at T_{MO} is almost pressure independent up to 2.51 GPa, the highest pressure in this experiment (see Fig. 11). Very close to p_c we observe at 1.48 GPa not only the magnetic anomaly, but also still the onset of a very broad superconducting anomaly. Similar coexistence of magnetism and superconductivity has been observed in Ref. [32] by ac calorimetry. At the border of an antiferromagnetic instability, it is difficult to observe a magnetic transition inside the superconducting state ($T_{MO} < T_{SC}$), whereas superconductivity occurs often inhomogeneously inside the magnetically ordered state when $T_{SC} < T_{MO}$. A very well-studied example for this competition of magnetic order and superconductivity is given by $CeRhIn_5$ [74,75] with the inhomogeneous appearance of superconductivity below its critical pressure ($T_{SC} < T_N$), followed by the rapid suppression of magnetic order above p_c when $T_{SC} > T_N$.

As shown in Fig. 10(b), ρ_c decreases with decreasing temperature for all pressures above 50 K. Similarly to the zero-pressure data, at low temperatures a pronounced maximum $T_{\rho_c}^{\max}$ occurs. This maximum shifts to lower temperatures with pressure up to 1.32 GPa. At this pressure, just below p_c, it almost coincides with the onset of superconductivity. The maximum of $T_{SC} \approx 3$ K is observed at 1.2 GPa for both samples. The normal-state resistivity changes drastically above the critical pressure p_c. At $p = 1.61$ GPa, ρ_c increases strongly below 10 K by a factor of 2, shows a small plateau below 7 K, and increases again below 3.45 K with a maximum at 2.4 K. The strong increase of the resistivity is attributed to a short-range magnetic order at $T_{WMO} \approx 7.5$ K and antiferromagnetic order below 3.5 K. A common feature between the a and c axes transport is the increase of the resistivity at the lower magnetic transition T_{MO}, which may indicate the opening of an electronic gap when entering in the magnetic state. The residual resistivity ρ_0 increases for both current directions strongly through p_c, and the anisotropy of the residual resistivity ρ_{c0}/ρ_{a0} is still of the order of three in the magnetically ordered state.

In Fig. 11 we summarize the pressure-temperature phase diagram of UTe_2 from the present resistivity measurements combined with previous studies [4,31]. The characteristic temperatures determined from the temperature dependence of the resistivity $T_{\rho_a}^{\max}$, $T_{\rho_c}^{\max}$, the maximum of the magnetic susceptibility measured along the b axis, $T_{\chi_b}^{\max}$, and $T_{\chi_a}^{\star}$, which marks a broad shoulder in the susceptibility measured along the a axis [31], decrease up to the critical pressure $p_c \approx 1.5$ GPa. $T_{\chi_a}^{\star}$ follows roughly $T_{\rho_c}^{\max}$. Recently, we have shown that $T_{\rho_a}^{\max}$ scales with the maximum of the magnetic susceptibility $T_{\chi_b}^{\max}$ [17,33] as a function of magnetic field and pressure, when a background contribution to the resistivity is subtracted. The background corresponds to the resistivity in the high-field regime above H_m, where the system is in a polarized state and magnetic fluctuations are strongly suppressed. The magnetic interactions change drastically at the critical pressure and for $p > p_c$, the crystallographic b axis becomes the axis of easy magnetization in the magnetic ordered state, while the a axis is an intermediate axis [31,34].

B. *c*-axis transport under pressure and in magnetic field $H \parallel b$

Next we focus on the c-axis resistivity ρ_c for field applied along the b axis at different pressures. Figure 12(a) shows the temperature dependence of ρ_c for different fields $H \parallel b$ at 0.35 GPa. Near $T_{\rho_c}^{\max} \approx 12$ K the resistivity shows a maximum which is slightly lower than at ambient pressure. Under magnetic field, like at $p = 0$ (see Fig. 2), the maximum shifts to lower temperatures and, at 27.5 T, we find $T_{\rho_c}^{\max} \approx 5.5$ K. Above $H_m = 29.5$ T, at 30 T and for higher fields, the temperature dependence of ρ_c changes significantly and instead of a maximum, a sharp drop of the resistivity is observed below 5 K. By further increasing the field, this anomaly is shifted to slightly higher temperatures. At low temperatures $\rho_c(T)$ has a

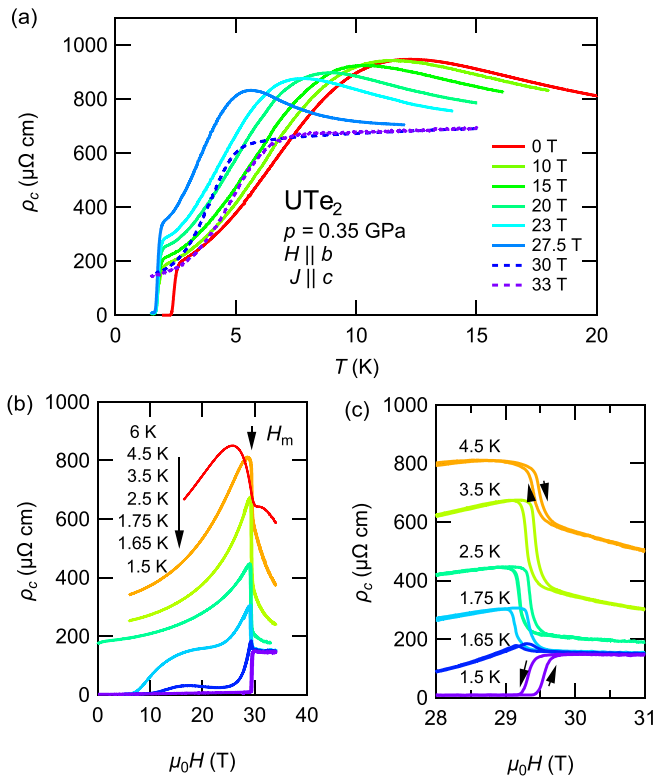

FIG. 12. (a) Temperature dependence of the resistivity at 0.35 GPa for different magnetic fields. Solid (dashed) lines are for fields below (above) the metamagnetic transition. (b) Field dependence of the resistivity for different temperatures. (c) Zoom on the magnetoresistivity around the metamagnetic transition.

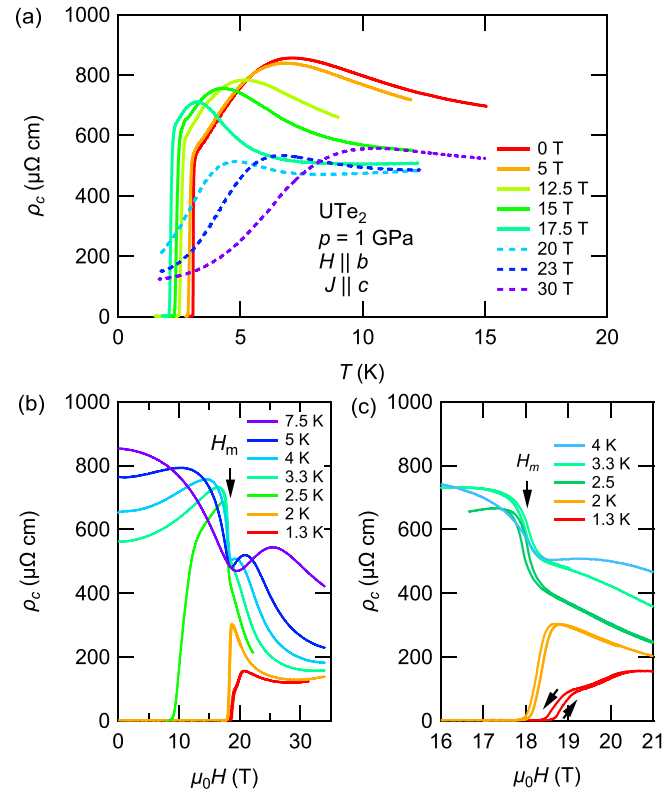

FIG. 13. (a) Temperature dependence of the resistivity at 1 GPa for different magnetic fields. Solid (dashed) lines are for fields below (above) the metamagnetic transition. (b) Field dependence of the resistivity for different temperatures. (c) Zoom on the magnetoresistivity around the metamagnetic transition.

T^2 temperature dependence in zero magnetic field up to 5 K, but with increasing field the T^2 range decreases significantly due to the low value of $T_{\rho_c}^{\max} \approx 5$ K. Even above H_m no clear T^2 is observed in the measured temperature range down to 1.5 K. The superconducting transition temperature decreases from $T_{\rm SC} = 2.28$ K at zero field down to $T_{\rm SC} = 1.65$ K at 8 T and is almost field independent in higher fields up to 27.5 T. Thus, the field enhancement of superconductivity is less pronounced compared to ambient pressure, but a phase line between the lfSC and hfSC phases still exists [27].

In Fig. 12(b) we show the field dependence $\rho_c(H)$ up to 35 T for different temperatures at $p = 0.35$ GPa. At the lowest temperature, superconductivity survives up to $H_m = 29.5$ T. A large jump to the normal-state resistivity occurs at H_m. $\rho_c(H)$ shows a hysteresis between the up and down sweeps of the field [see Fig. 12(c)] indicating the first-order nature of the transition at H_m. At 1.65 K, the signature of the first-order metamagnetic transition is very weak. At higher temperatures, we observe a marked hysteresis at the metamagnetic transition and the magnetoresistance $\rho_c(H)$ decreases strongly. At 6 K no hysteresis is observed anymore, indicating that the critical point of the first-order transition is located between 4.5–6 K, thus lower than at ambient pressure.

Figures 13 and 14 show the resistivity for higher pressures (1 and 1.32 GPa, respectively) approaching the critical pressure. From the magnetoresistance at 1 GPa we conclude that the metamagnetic transition field is further reduced down to $\mu_0 H_m = 18.5$ T [see Fig. 13(b)]. The temperature dependence of the resistivity has changed slightly compared to lower pressures, and only the characteristic temperatures are lower. The maximum in $\rho(T)$ decreases from $T_{\rho_c}^{\max} = 7.5$ K at $H = 0$ to 3.24 K at $\mu_0 H = 17.5$ T. For fields above H_m the absolute value of the resistivity has decreased and a shallow maximum in the temperature dependence appears at 4.8 K at 20 T. This maximum shifts to higher temperatures with increasing magnetic field. The superconducting transition is monotonously suppressed from 3.05 K at $H = 0$ to 2.07 K at 17.5 T. Due to the high superconducting transition temperature and to the low $T_{\rho_c}^{\max}$, no T^2 temperature dependence is observed in the normal state above the superconducting transition. A Fermi-liquid T^2 dependence is only recovered above the metamagnetic transition in the polarized phase for fields above H_m, but the maximum temperature is about 3.5 K, thus the T^2 regime is very narrow. We observe zero resistivity up to H_m at 1.3 and 2 K [see Figs. 13(b) and 13(c)]. We do not find any signature of a reinforcement of superconductivity, but the upper critical field is monotonously suppressed.

In the normal state a maximum develops in the magnetoresistance at temperatures higher than the critical point, which is near 3.5 K and 17.5 T at 1 GPa. The maximum shifts to higher temperatures with increasing magnetic fields.

Figure 14 presents the temperature and field dependence of ρ_c close to the critical pressure at 1.32 GPa. At zero magnetic

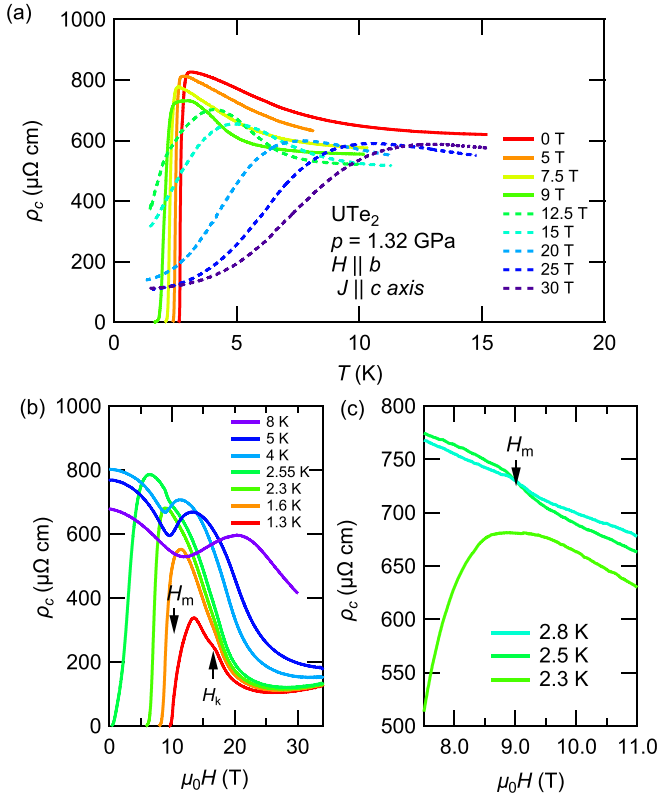

FIG. 14. (a) Temperature dependence of the resistivity at 1.32 GPa for different magnetic fields. Solid (dashed) lines are for fields below (above) the metamagnetic transition. (b) Field dependence of the resistivity for different temperatures. (c) Zoom on the magnetoresistivity around the metamagnetic transition.

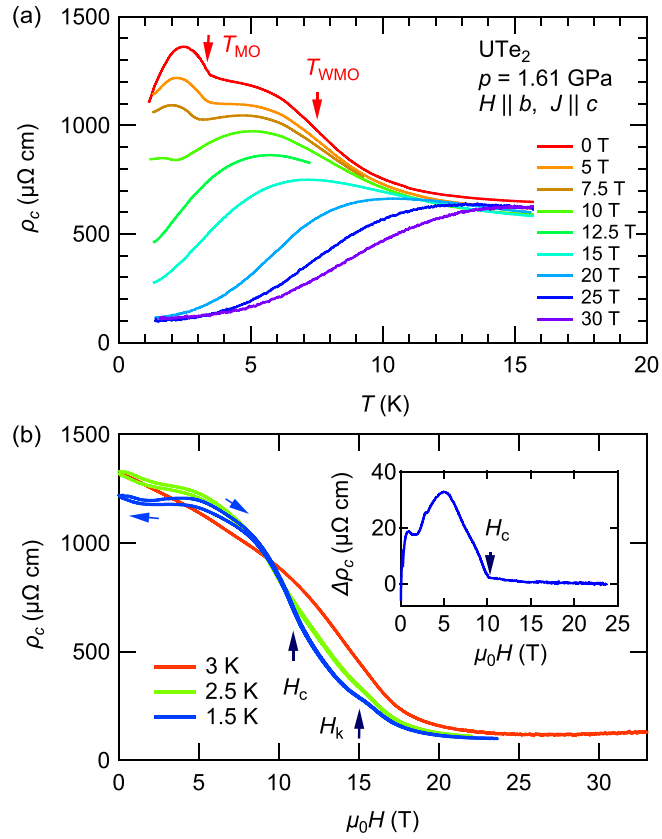

FIG. 15. (a) Temperature dependence of the resistivity at 1.61 GPa for different magnetic fields. T_{MO} indicates the magnetic ordering temperature and T_{WMO} the crossover to a short-range correlated regime at zero field, respectively. (b) Field dependence of the resistivity for different temperatures measured at the LNCMI. Blue arrows indicate the direction of the field sweep. H_c and H_k mark the critical field of the disappearance of the hysteresis and a well-defined kink in the magnetoresistivity at 1.5 K. The inset in (b) shows the difference $\Delta\rho_c$ between field-up and field-down sweeps at 1.5 K, with the opening of the hysteresis at $H_c = 10.3$ T.

field the resistivity increases with decreasing temperature, superconductivity sets in near 3 K and zero resistivity is attained at 2.65 K. The shallow maximum near 3.05 K at zero field may already be a signature of the onset of superconductivity. The characteristic temperature $T_{\rho_c}^{\max}$ seems to be lower or at most of the same order than T_{SC}. Under magnetic field up to 9 T a shallow maximum occurs just above the onset of superconductivity. Above $H \approx 9$ T, close to H_m, a broad maximum in $\rho_c(T)$ occurs and is shifted to higher temperatures for higher magnetic fields. At low temperatures a Fermi-liquid regime occurs.

The field dependence $\rho_c(H)$ is shown in Fig. 14(b) for different temperatures. Figure 14(c) displays the field range around the metamagnetic transition in an enlarged scale. We first discuss $\rho(H)$ at the lowest temperature $T = 1.3$ K [see Fig. 14(b)]. Zero resistivity is observed up to ≈9.6 T in the field sweep with increasing field. For higher fields the resistivity increases sharply and has a change of slope as a function of field near 10.15 T. A clear signature of the metamagnetic transition is missing. By further increasing the field, $\rho_c(H)$ at 1.3 K has a maximum at 13.3 T, which marks the onset of superconductivity near H_{c2} in the field sweep. A well-defined kink in $\rho_c(H)$ occurs at $H_k = 17.1$ T in the normal state. For even higher fields the magnetoresistivity has a minimum around 26 T. With increasing temperature these features get broadened and the kink cannot be followed above 2 K. Figure 14(c) displays the anomaly of the metamagnetic transition on an enlarged scale. While at 2.3 K almost no anomaly at the metamagnetic transition occurs due to the closeness to the onset of superconductivity (at 8.7 T), at 2.5 and 2.8 K only a tiny anomaly indicates the metamagnetic transition; no jump or marked decrease in $\rho_c(H)$ occurs anymore. Therefore, the critical point of the first-order transition can no longer be resolved due to superconductivity. For temperatures above 2.8 K no signature of H_m is detected. At 4 K the magnetoresistivity shows a minimum at 9 T and a maximum at 11.4 T. This maximum shifts to higher fields with increasing temperature, similarly to the temperature $T_{\rho_c}^{\max}$ of the maximum in $\rho_c(T)$ at fixed field.

Finally, in Figs. 15 and 16 we show the temperature and field dependencies of c-axis resistivity at $p = 1.61$ GPa. On cooling, the resistivity shows a smooth increase at zero field below 10 K with an inflection point at $T_{WMO} \approx 7.5$ K, and a sharp increase at $T_{MO} = 3.45$ K. Under field, T_{WMO} increases slightly in temperature up to 10 T, and much faster for higher fields when it gets less pronounced, (Fig. 25 in the Appendix which shows $d\rho/dT$ for different magnetic fields). On the

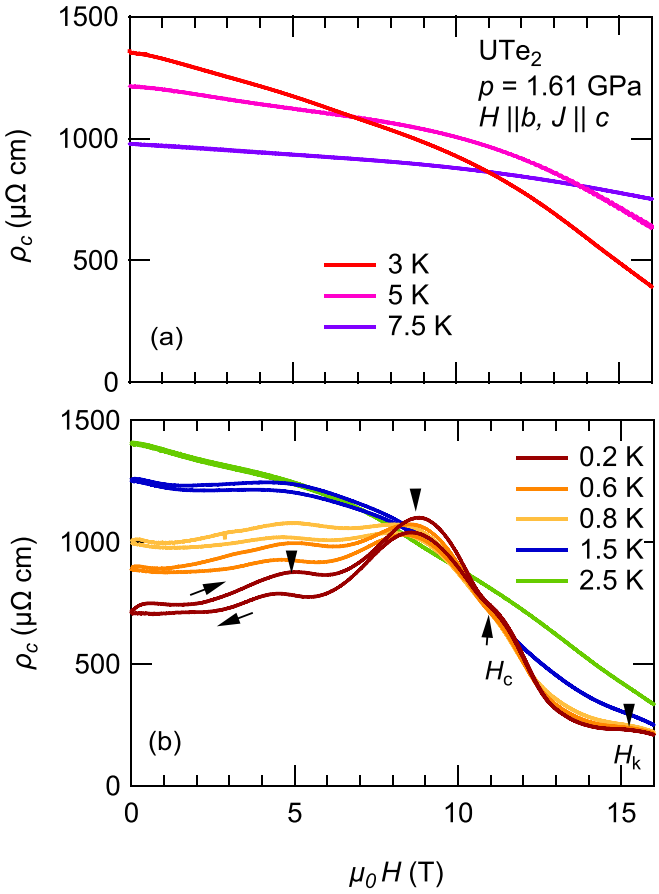

FIG. 16. Field dependence of the c-axis resistivity at 1.61 GPa for different temperatures above (a) and below T_M (b). A strong hysteresis occurs in the magnetic state. H_c indicates the critical field of the magnetic order. H_k indicates a kink in the resistivity (see also Fig. 15).

contrary, T_{MO} decreases with increasing field, and its signature stays sharp under field up to 10 K.

A strongly negative magnetoresistance up to fields of 30 T is visible in Fig. 15(b). It decreases by more than a factor 10 from zero field to 20 T, indicating the suppression of the magnetic scattering related to the magnetic correlations established below the characteristic temperature T_{WMO}. This strong magnetoresistance at low temperatures contrasts with the rather low variation of the magnetoresistance by only 2% at 15 K. For temperatures above T_{MO} the magnetoresistance does not show any hysteresis and decreases monotonously below 20 T. On the contrary, below T_{MO} the magnetoresistance shows a significant hysteresis for field-up and field-down sweeps. We define the field H_c, where the hysteresis disappears, as the critical field of the magnetically ordered state (see inset in Fig. 15). H_c determined here from the field sweeps coincides with the temperature T_{MO} determined from the temperature sweeps. Inside the magnetically ordered state several additional anomalies occur. In Figs. 15(b) and 16(b) maxima of the magnetoresistance are found in fields $H < H_c$. These findings are similar to those reported in Refs. [27,33]. The observation of clear anomalies in the magnetic ordered state is presumably an indication for reorientations of the magnetic moments inside the magnetically ordered state. Of course, thermodynamic measurements are needed to determine the phase lines inside the ordered state. Very recently, an incommensurate antiferromagnetic order has been observed by neutron diffraction experiments [30].

For fields $H > H_c$ we observe at low temperatures an additional kink at H_k in the magnetoresistance. A similar feature had been already observed at lower pressures in the polarized state at $p = 1.32$ GPa. The signature of H_k disappears for temperatures above 3 K. A comparable kink in the magnetoresistance has been observed for an angle of 25° from the b toward the c axis at about 21 T [76]. The origin of this anomaly is still an open question.

C. Discussion of the pressure dependence

Figure 17 summarizes the H-T phase diagrams at different pressures determined from the resistivity measurements with current $J \parallel c$ and field $H \parallel b$. For all pressures below p_c, $T_{\rho_c}^{\max}$ is connected to the metamagnetic transition. Superconductivity is observed up to H_m, which decreases with pressure. For fields higher than H_m a crossover to a polarized regime occurs as a function of temperature. Close to the critical pressure an additional kink occurs in the polarized state at low temperatures in $\rho_c(H)$ at H_k, which persists also above p_c. Above the critical pressure, at 1.61 GPa, two magnetic anomalies occur: the lower anomaly T_{MO} is a transition to a long-range magnetically ordered state. Its antiferromagnetic nature was suggested by the different phase lines inside the ordered state and has been recently shown by neutron diffraction under high pressure [30]. On the contrary, the presence of a true phase transition at T_{WMO} is less clear, and not only broad features occurs in the resistivity, but also in magnetization [31] or specific-heat measurements [32]. The field dependence of $T_{\mathrm{WMO}}(H)$ resembles that of a ferromagnet under field applied along the easy magnetization axis, as the transition at T_{WMO} smears out under a magnetic field and shifts to higher temperatures in a similar way as the maximum $T_{\rho_c}^{\max}$. However, the microscopic origin of T_{WMO} has not been identified today, and crystal-field effects may also be not negligible. We recall that the magnetic anisotropy changes at p_c with b being the easy and c the hard magnetization axis [31]. The coexistence and competition of antiferromagnetic and ferromagnetic fluctuations has been suggested from NMR measurements [77].

The pressure evolution of the superconducting phase diagram is similar to those previously discussed in Ref. [4] and shown in Fig. 18. The superconducting transition temperature increases with applied pressure and superconductivity is stable under magnetic field up to the metamagnetic transition, but the temperature dependence of the upper critical field $H_{c2}(T)$ changes significantly under pressure. At low pressure (see at 0.35 GPa) a reinforcement of superconductivity under magnetic field can still be observed. The critical field $H^\star$ of the upturn of $H_{c2}(T)$ is already strongly reduced from about 17 T at zero pressure to around 8 T at 0.35 GPa. The pressure 0.35 GPa is very close to the pressure, where ac calorimetry at zero field indicates two different superconducting phases [25,28,32]. Previous reports of the upper critical field for $H \parallel b$ [4,27] in that pressure range show at low field a concave curvature, indicating the increase of pairing strength under

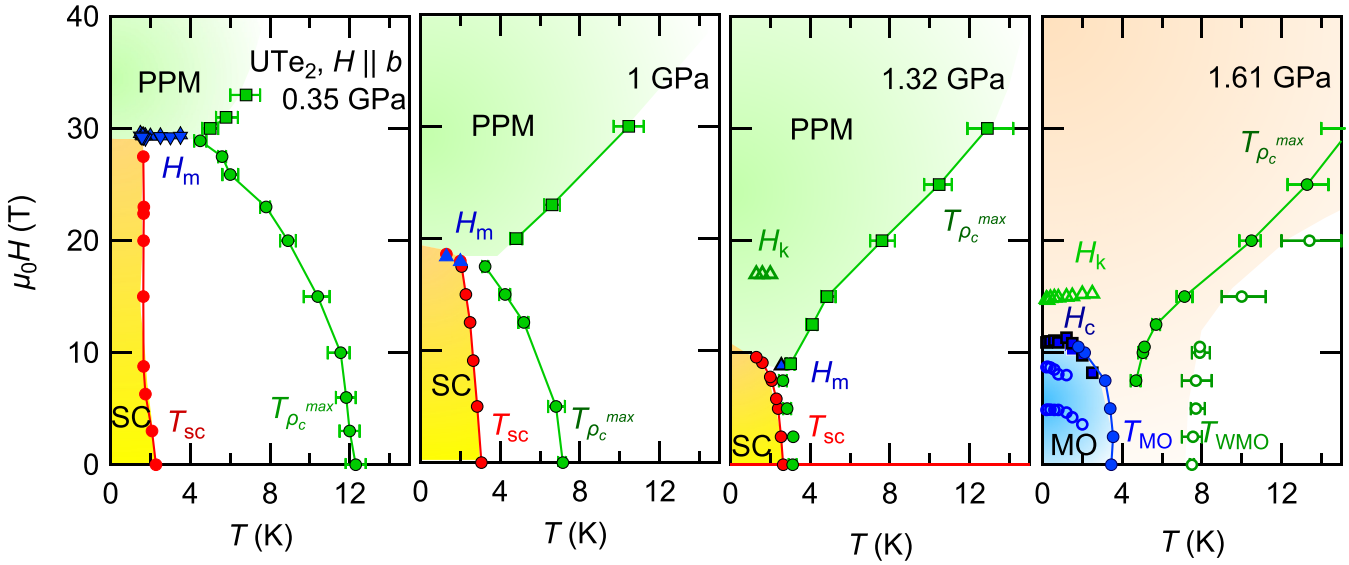

FIG. 17. Magnetic and superconducting phase diagram of UTe_2 at 0.35, 1.1, 1.32, and 1.61 GPa for field applied along the b axis defined from the resistivity measurements with $J \parallel c$. Full green circles (squares) indicate the maximum of the resistivity $T_{\rho_c}^{\max}$ as function of temperature below (above) the metamagnetic transition. The superconducting transition at $T_{SC}(H)$ (full red circles) is defined by zero resistivity. The metamagnetic transition at H_m is marked by blue triangles for pressures below $p_c \approx 1.45$ GPa. SC marks the superconducting phase, PPM the polarized paramagnetic phase above H_m. At 1.61 GPa long-range magnetic order (MO) occurs below T_{MO} up to H_c. T_{WMO} (open circles) is defined by the inflection point of the increase of the c-axis resistivity and shows a similar field dependence as the maximum of the resistivity $T_{\rho_c}^{\max}$. No metamagnetism occurs. Open blue circles (determined from extrema of the magnetoresistivity) correspond probably moment reorientations in the MO state. H_c indicates the critical field for the magnetically ordered state. H_k indicates the kink in the magnetoresistivity in the polarized high-field regime.

magnetic field. As initially T_{SC} decreases with increasing pressure, the data at 0.35 GPa suggest that for this pressure already two superconducting phases should exist since T_{SC} is higher than at zero pressure. Thus, on cooling at zero magnetic field we should enter first in a high-temperature superconducting phase. Of course, with resistivity measurements, it is not possible to discern different superconducting phases and detect phase lines inside a superconducting phase. The critical temperature T_{SC} determined by resistivity measurements is always that of the phase with the higher T_{SC}. In Refs. [27,78] it has been proposed that the lfSC is suppressed with pressure and

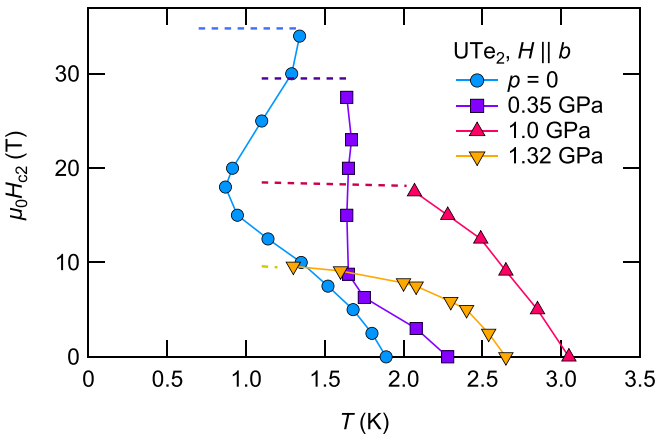

FIG. 18. Superconducting upper critical field H_{c2} for different pressures. Dashed lines indicate the metamagnetic field for each pressure, which is the upper field limit of superconductivity.

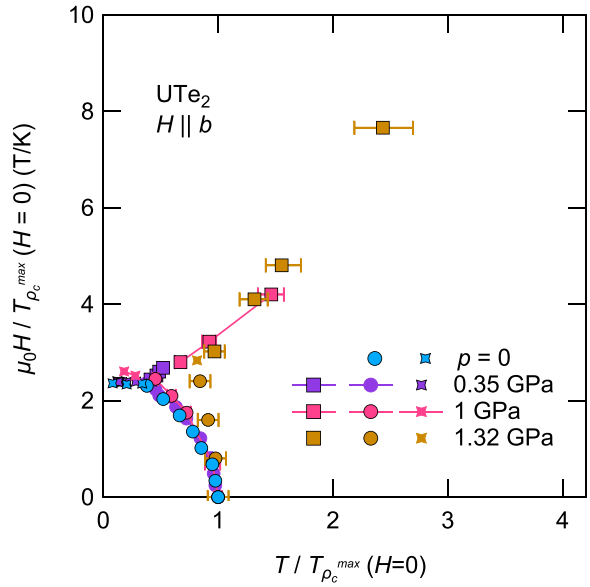

FIG. 19. Magnetic phase diagram of UTe_2 for field along the b axis normalized to the temperature $T_{\rho_c}^{\max}(H=0)$ at zero magnetic field as a function of the normalized temperature. Circles (squares) give $T_{\rho_c}^{\max}$ below (above) the metamagnetic transition, stars indicate $H_m(T)$ for the different pressures.

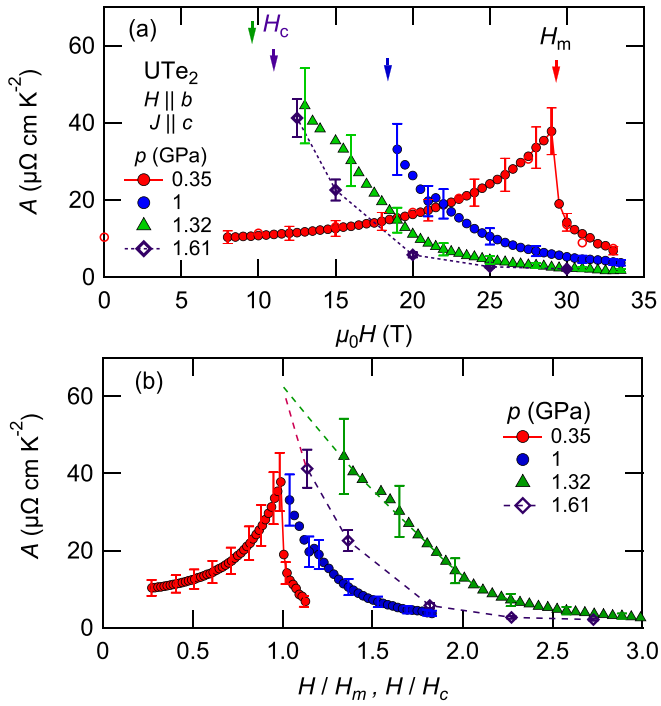

FIG. 20. (a) A coefficient as a function of magnetic field. Solid arrows indicate the position of H_m for the different pressures, the dashed arrow the critical field of the magnetic order. Due to the closeness of $T_{\rho_c}^{\max}$ and T_{SC}, A can be only determined at 1 and 1.32 GPa for $H > H_m$, where superconductivity is suppressed. Above the critical pressure at 1.61 GPa a Fermi liquid is only observed for fields above H_c. Dashed lines are guides to the eye. (b) A as a function of the normalized field, H_m for $p < p_c$ and H_c for $p > p_c$. Lines are guides to the eye.

embedded in the high-temperature superconducting phase. The high-temperature superconducting phase is proposed to be the pressure continuation the hfSC.

More detailed studies by thermodynamic probes of the phase line between the lfSC and hfSC phases for $H \parallel b$ are needed in future. They should be performed in the vicinity of the pressure where the high-temperature superconducting phase appears and under magnetic field applied along b.

Obviously, the temperature dependence of H_{c2} changes on approaching p_c. At $p = 1$ GPa we do not observe any signature of a field enhancement of superconductivity up to H_m in agreement with previous studies [4,27]. The strong curvature of $H_{c2}(T)$ might indicate the increase of the paramagnetic limitation near p_c for $H \parallel b$ [4]. The question of the pairing symmetry of the superconducting state near p_c is still open. On one side, the NMR Knight shift stays constant on cooling through T_{SC} favoring an odd-parity pairing. On the other side, if the high-temperature superconducting phase corresponds to the pressure evolution of the hfSC state, it could also be a singlet state. In Ref. [8] it has been proposed that the hfSC may be spin singlet and driven by critical fluctuations on approaching the metamagnetic transition. Under pressure, the hfSC state may survive up to p_c. It has even been predicted [79] that antiferromagnetic fluctuations would be reinforced under pressure, favoring a spin-singlet state for the high-temperature superconducting phase above 0.3 GPa. As the magnetically ordered state MO is antiferromagnetic, antiferromagnetic fluctuations may drive the superconductivity close to the critical pressure. However, even at ambient pressure and low field the pairing mechanism in UTe_2 is still not settled.

Next we will concentrate on the normal-state properties. As shown in Fig. 17 the temperature $T_{\rho_c}^{\max}$ of the maximum in the c-axis resistivity is decreasing with applied pressure. For all pressures below p_c the field dependence of $T_{\rho_c}^{\max}$ connects to the metamagnetic transition H_m, where $T_{\rho_c}^{\max}$ has its lowest value. For fields above H_m, $T_{\rho_c}^{\max}$ marks the crossover to a polarized paramagnetic regime. If we identify the minimum value of $T_{\rho_c}^{\max}$ as the critical point of the first-order metamagnetic transition, we determine that this critical point decreases almost linearly with pressure from about (5.6 K, 34 T) at zero pressure to (2.55 K, 8.85 T) at 1.32 GPa. At 1.32 GPa the signature of the metamagnetic transition is almost lost and only a tiny anomaly is visible.

In Fig. 19 we plot the phase diagram of the normal state scaled in field and temperature by the temperature $T_{\rho_c}^{\max}(H = 0)$. Importantly, the phase diagrams of the different pressures below p_c scale almost perfectly. Only for $p = 1.32$ GPa the scaling is less good, but this may be due to the difficulty to determine $T_{\rho_c}^{\max}$ at low field correctly due to the high superconducting temperature $T_{SC} \approx T_{\rho_c}^{\max}$. Our thermal expansion measurements at zero pressure clearly show the correspondence $T^\star \approx T_\alpha^\star \approx T_{\rho_c}^{\max} \approx 14.5$ K. This characteristic temperature scale connects to the metamagnetic transition at H_m. The microscopic origin of $T^\star$ is clearly related to the interplay of magnetic fluctuations and the formation of a coherent heavy-fermion state. This has been shown by different NMR and also inelastic neutron scattering experiments at ambient pressure. Inelastic neutron scattering evidenced the development of antiferromagnetic fluctuations at wave vector $\mathbf{k_1} = (0, 0.57, 0)$ below 60 K which saturate below 15 K [52–54]. The magnetic fluctuations in UTe_2 depend strongly on the particular ladderlike structure of the U atoms along the a axis with the rung along the c axis. Two-dimensional antiferromagnetic fluctuations originating from magnetic ladders coupled along b were captured by inelastic neutron scattering and have a characteristic energy scale of 3–4 meV. The temperature dependence of these fluctuations is compatible with that from the NMR relaxation rate $1/T_1T$ [51,80]. Under pressure, $1/T_1T$ measured on the different Te sites also show a constant behavior up to $T^\star$ [34,77] and $T^\star$ from the NMR scales with $T_{\rho_c}^{\max}$ determined from the resistivity. This seems to be the dominant energy scale which determines the pressure and field dependence of the phase diagram.

We emphasize that electronic correlations increase on approaching the critical pressure. The field dependence of the A coefficient from our measurements with a current along the c axis is shown in Fig. 20(a) as a function of the field and in Fig. 20(b) as a function of the normalized field H/H_m ($p < p_c$) or H/H_c ($p > p_c$). (Figures 26 and 27 in the Appendix show the experimental data and the corresponding fits.) At 0.35 GPa $A(H)$ has still a similar field dependence as at ambient pressure and A shows a steplike decrease just above the metamagnetic transition. For higher pressures, due to the

lower $T_{\rho_c}^{\max}$, the onset of superconductivity prevents the determination of A below the metamagnetic transition in ρ_c. Thus, $A(H)$ has been only determined in the field range above H_c. It shows a strong monotonous decrease. The enhancement of the A coefficient at H_m is the largest close to the critical pressure and comparable to A on approaching H_c in the magnetic state. This indicates that quantum criticality in UTe_2 is important for the formation of the antiferromagnetic state. This leads to the enhancement of superconductivity under magnetic field close to the critical pressure and to the reentrant behavior of superconductivity along the c axis [33,35]. However, the transition from the superconducting ground state to the magnetically ordered may be first order and connected to a strong change in the electronic structure. Indication for this is the abrupt increase in the residual resistivity through p_c [35,81]. Direct microscopic evidence for this is given by the change by 7% of the $5f$ count through p_c towards the U^{4+} configuration [81]. As already mentioned, this change in the electronic structure goes along with a drastic change in the magnetic anisotropy.

V. CONCLUSIONS

We have shown that the resistivity in UTe_2 depends strongly on the electrical current direction. The measurements with $J \parallel c$ clearly reveal the important energy scales. In particular, at the metamagnetic transition at $\mu_0 H_m \approx 34.5$ T the resistivity ρ_c strongly decreases for current applied along the c axis, while ρ_a and ρ_b strongly increase (current along a or b axis, respectively). The field dependence of the A coefficient for $J \parallel c$ seems to replicate $\gamma(H)$ better than for the other current directions. The maximum $T_{\rho_c}^{\max}$ in the temperature dependence of ρ_c decreases on approaching the critical point of the first-order metamagnetic transition line. $T_{\rho_c}^{\max}$ coincides with the temperature of the minimum observed in the thermal expansion α_b along the b axis. Under hydrostatic pressure $T_{\rho_c}^{\max}$ and H_m decrease up to the critical pressure p_c. The phase diagram in the normal state below p_c scales with $T_{\rho_c}^{\max}$, indicating the importance of this low-energy scale: the coherence along the c axis governs the low-temperature behavior. Superconductivity is observed for all pressures up to H_m, which collapses at p_c. At zero pressure the low-field superconducting phase scales with T_{SC} independently of the sample quality, while the high-field superconducting phase is strongly sample dependent. This indicates that these two phases may emerge from different pairing mechanisms [8]. Accurate determination of the phase diagrams under pressure by thermodynamic measurements under magnetic field along the b axis are strongly required, in particular, close to the pressure where the high-temperature superconducting phase occurs. This will elucidate whether the high-temperature superconducting phase is the pressure evolution of the field-induced hfSC phase, or not. A future challenge will be to specify the field and pressure dependence of the valence and spin correlations and their feedback on superconductivity under pressure.

ACKNOWLEDGMENTS

We thank K. Ishida, Y. Yanase, and M. E. Zhitomirsky for fruitful discussions. We received financial support from the French Research Agency ANR within the projects FRESCO, Project No. ANR-20-CE30-0020, and FETTOM, Project No. ANR-19-CE30-0037. Further financial support has been provided by the JPSJ programs KAKENHI Grants No. P22H04933, No. JP20K20889, No. JP20H00130, and No. JP20KK0061. We acknowledge support of the LNCMI-CNRS, member of the European Magnetic Field Laboratory (EMFL) and from the Laboratoire d'exellence LANEF (Grant No. ANR-10-LABEX-51-01).

APPENDIX

In the Appendix, we show additional figures to which we refer in the main text and which supports the analysis of the data. Figure 21(a) shows the magnetoresistance ρ_c for field

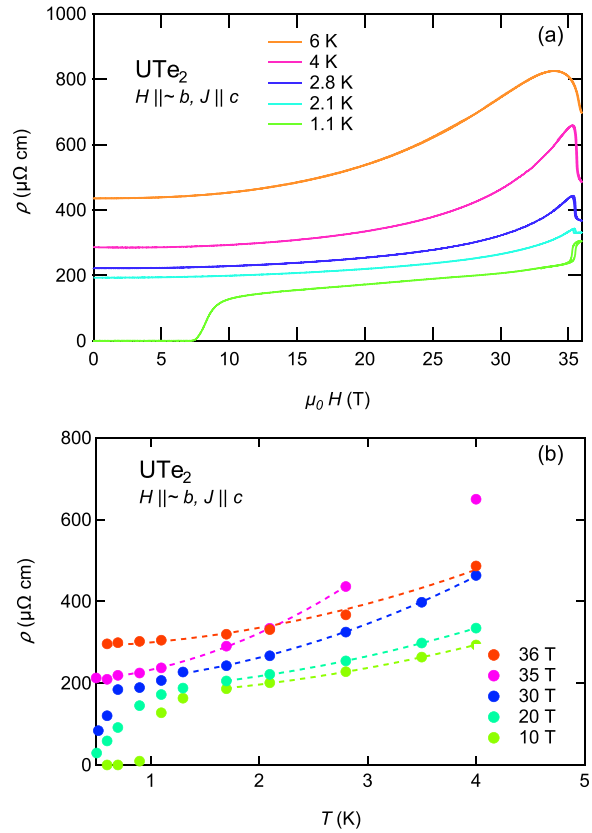

FIG. 21. (a) Magnetoresistance ρ_c for field $H \parallel\sim b$ and current along c measured on sample S5 for different temperatures T between 1 and 6 K. The metamagnetic transition appears at $H_m = 35.4$ T in the field-up sweeps. The hysteresis of the metamagnetic transition is about 0.4 T. While for $T = 1.1$ K the jump at H_m is positive, it is negative and very tiny at 2.1 K when the sample is in the normal state for all fields. The lower panel (b) shows the temperature dependence extracted from the field-dependent measurements. Fermi-liquid fits (dashed lines) are performed in the temperature range $T < 4$ K.

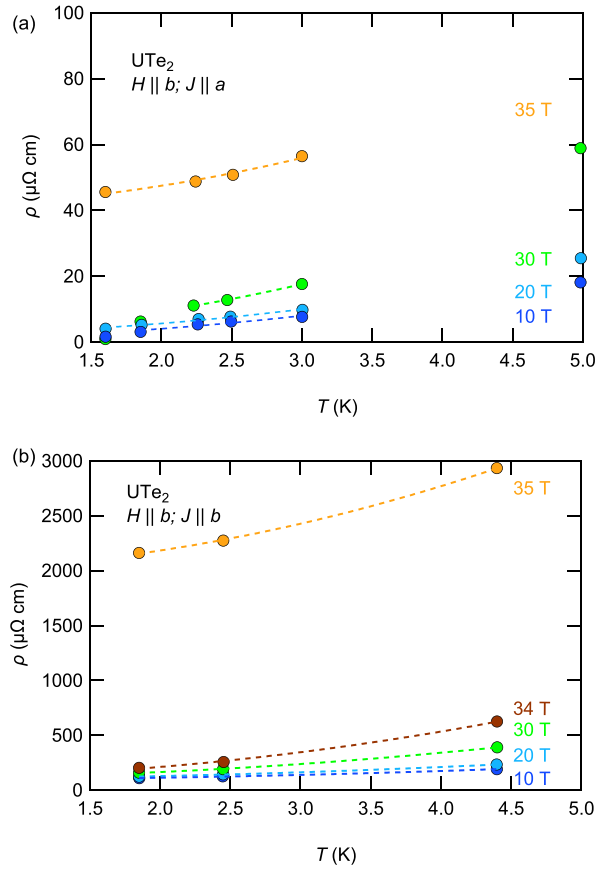

FIG. 22. (a) Temperature dependence of the resistivity for different magnetic fields reconstructed from the magnetoresistance measurements show for field $H \parallel\sim b$ measured on sample S3 for $J \parallel a$ (upper panel) and on sample S4 for $J \parallel b$ (lower panel). T^2 fits are indicated by the dotted lines, due to the limited temperatures error bars for the A coefficient shown in Fig. 7 are rather large.

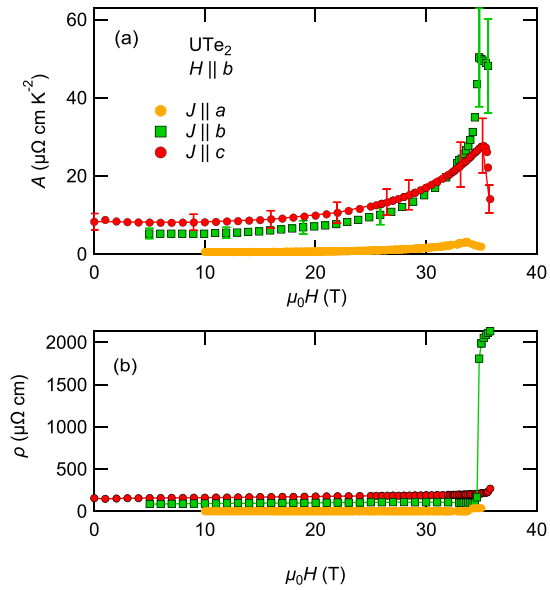

FIG. 23. (a) Fermi-liquid coefficient A as a function of the magnetic field $H \parallel b$ with current J applied along a, b, and c axes. (b) Field dependence of the residual resistivity rho_0 for the different current directions.

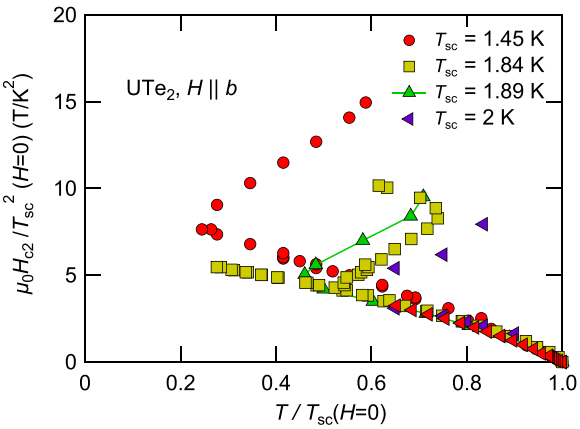

FIG. 24. Upper critical field H_{c2} normalized by T_{SC}^2 versus T/T_{SC} for the different samples. This scaling would correspond to a purely orbital limited upper critical field. However, the scaling of the critical field only by T_{SC} shown in Fig. 9 seems to be better.

$H \parallel\sim b$ and current along c measured on sample S5 for different temperatures T between 1 and 6 K. The metamagnetic transition appears at $H_m = 35.4$ T in the field-up sweep. In addition, the field reentrance of superconductivity does not occur above $H^\star$. This indicates that the sample has not been perfectly aligned along the b axis. However, the normal state properties are much less dependent on the perfect alignment. In Fig. 21(b) we plot the temperature dependence of the resistivity determined from the field-dependent measurements at constant temperature. The dashed ρ_0 lines give the fits with a Fermi-liquid temperature dependence $\rho = \rho_0 + AT^2$. The T^2 temperature dependence holds up to 4 K, only close to H_m is the upper limit of the T^2 range lower. The field dependence of A and the residual resistivity ρ_0 are displayed in Fig. 7 in the main text.

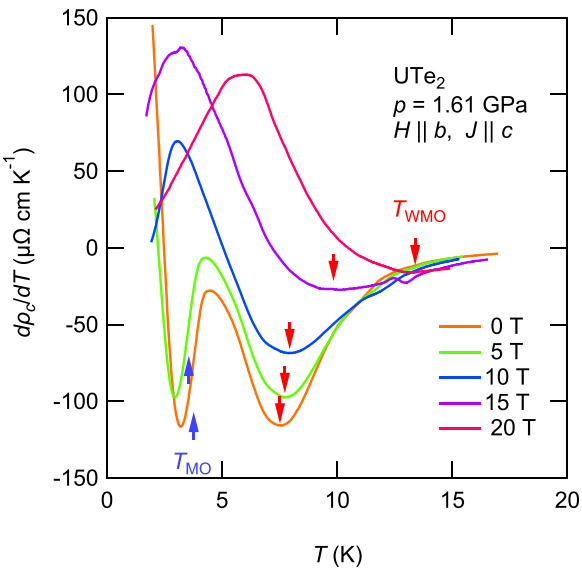

FIG. 25. Temperature derivative $d\rho_c/dT$ at $p = 1.61$ GPa for different magnetic fields. The arrows indicate the magnetic transition temperature T_{MO} and the temperature of the crossover T_{WMO}.

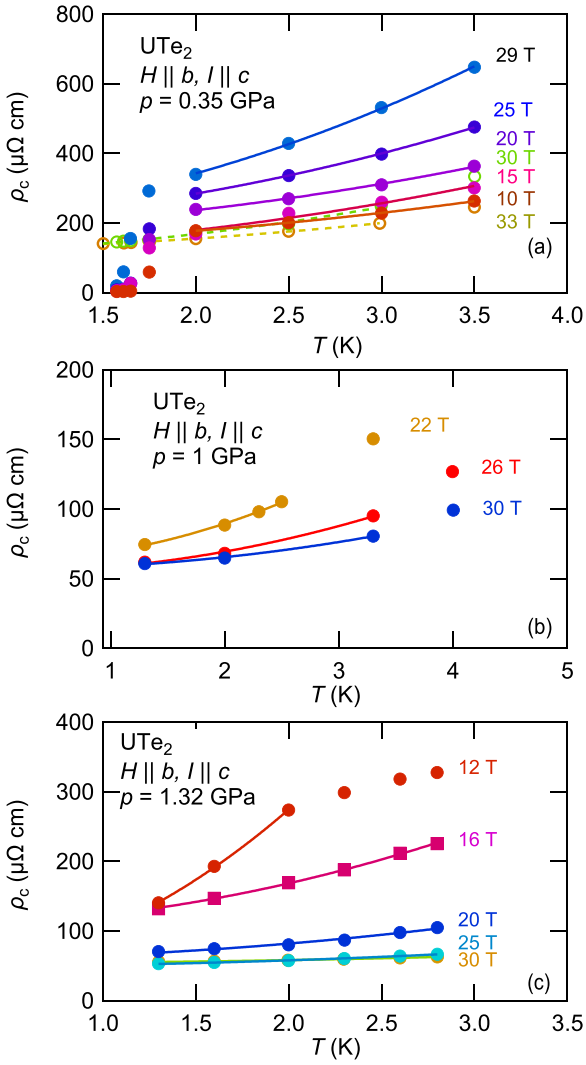

FIG. 26. Temperature dependence of the resistivity reconstructed from the measured magnetoresistance for different magnetic fields for different pressures (a) 0.35 GPa, (b) 1 GPa, and (c) 1.32 GPa.

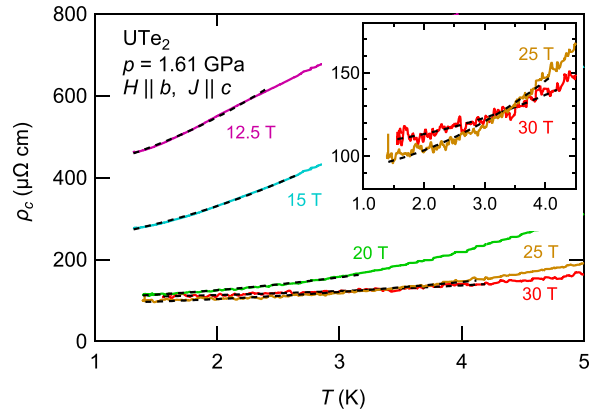

FIG. 27. Temperature dependence of the resistivity ρ_c at 1.61 GPa as a function of temperature up to 5 K for different magnetic fields in the polarized magnetic regime above the critical field H_c of the antiferromagnetic state. The dashed lines indicate fits with a Fermi-liquid temperature dependence $\rho_c = \rho_0 + AT^2$. The temperature range of the Fermi-liquid range decreases strongly on approaching H_c. The inset shows the data at 25 and 30 T in an expanded view.

In Fig. 22 we show the temperature dependence of the resistivity for different magnetic fields for the current applied along the a axis (a) and b axis (b). The temperature dependence has been reconstructed from field-dependent measurements at constant temperatures. The A coefficient has been determined from Fermi-liquid fits and is reported in Fig. 7 of the main text in a normalized representation. Figure 23 presents the A coefficient and ρ_0 for the different current directions in absolute units.

In Fig. 9(b) of the main text we have shown the upper critical field H_{c2} measured for different samples with different values of the superconducting transition T_{sc} normalized by the value of T_{sc}. In Fig. 24 we plot the upper critical field H_{c2} normalized by T_{sc}^2 versus T/T_{sc} for the different samples. This scaling would correspond to a purely orbital limited upper critical field. However, the scaling of the critical field only by T_{sc} shown in Fig. 9 seems to be better which show that a simple model cannot represent the temperature dependence of the upper critical field.

In Fig. 15 of the main text we have shown the temperature dependence of the resistivity at 1.61 GPa for different magnetic fields. In Fig. 25 of this Appendix we present the temperature derivative $d\rho_c/dT$ at 1.61 GPa for different magnetic fields. In this presentation it is clear that the temperature T_{WMO} increases with increasing magnetic field. We have identified T_{WMO} as the onset of weakly magnetic order, but the microscopic determination of the order is still missing.

In the following Figs. 26 and 27 we present the Fermi-liquid fits of the resistivity for different magnetic fields at different pressures. For the pressures 0.35, 1, and 1.32 GPa the A coefficient has been determined from the measured magnetoresistivity at constant temperatures which is shown in Fig. 26.

Figure 27 displays the temperature dependence of the resistivity at 1.61 GPa (see Fig. 15(a) in the main text) in an enlarged view at low temperatures. The dashed lines are T^2 Fermi-liquid fits. The A coefficient for the different pressures is shown in Fig. 20 of the main text.

[1] S. Ran, C. Eckberg, Q.-P. Ding, Y. Furukawa, T. Metz, S. R. Saha, I.-L. Liu, M. Zic, H. Kim, J. Paglione, and N. P. Butch, Nearly ferromagnetic spin-triplet superconductivity, Science **365**, 684 (2019).

[2] D. Aoki, A. Nakamura, F. Honda, D. Li, Y. Homma, Y. Shimizu, Y. J. Sato, G. Knebel, J.-P. Brison, A. Pourret, D. Braithwaite, G. Lapertot, Q. Niu, M. Vališka, H. Harima, and J. Flouquet, Unconventional superconductivity in heavy fermion UTe_2, J. Phys. Soc. Jpn. **88**, 043702 (2019).

[3] D. Aoki, J.-P. Brison, J. Flouquet, K. Ishida, G. Knebel, Y. Tokunaga, and Y. Yanase, Unconventional superconductivity in UTe_2, J. Phys.: Condens. Matter **34**, 243002 (2022).

[4] G. Knebel, M. Kimata, M. Vališka, F. Honda, D. X. Li, D. Braithwaite, G. Lapertot, W. Knafo, A. Pourret, Y. J. Sato, Y. Shimizu, T. Kihara, J. P. Brison, J. Flouquet, and D. Aoki, Anisotropy of the upper critical field in the heavy-fermion superconductor UTe_2 under pressure, J. Phys. Soc. Jpn. **89**, 053707 (2020).

[5] G. Nakamine, K. Kinjo, S. Kitagawa, K. Ishida, Y. Tokunaga, H. Sakai, S. Kambe, A. Nakamura, Y. Shimizu, Y. Homma, D. Li, F. Honda, and D. Aoki, Anisotropic response of spin susceptibility in the superconducting state of UTe_2 probed with ^{125}Te -NMR measurement, Phys. Rev. B **103**, L100503 (2021).

[6] H. Fujibayashi, G. Nakamine, K. Kinjo, S. Kitagawa, K. Ishida, Y. Tokunaga, H. Sakai, S. Kambe, A. Nakamura, Y. Shimizu, Y. Homma, D. Li, F. Honda, and D. Aoki, Superconducting order parameter in UTe_2 determined by Knight shift measurement, J. Phys. Soc. Jpn. **91**, 043705 (2022).

[7] H. Matsumura, H. Fujibayashi, K. Kinjo, S. Kitagawa, K. Ishida, Y. Tokunaga, H. Sakai, S. Kambe, A. Nakamura, Y. Shimizu, Y. Homma, D. Li, F. Honda, and D. Aoki, Large reduction in the a-axis Knight shift on UTe_2 with $T_c = 2.1$ K, J. Phys. Soc. Jpn. **92**, 063701 (2023).

[8] A. Rosuel, C. Marcenat, G. Knebel, T. Klein, A. Pourret, N. Marquardt, Q. Niu, S. Rousseau, A. Demuer, G. Seyfarth, G. Lapertot, D. Aoki, D. Braithwaite, J. Flouquet, and J. P. Brison, Field-induced tuning of the pairing state in a superconductor, Phys. Rev. X **13**, 011022 (2023).

[9] G. Knebel, W. Knafo, A. Pourret, Q. Niu, M. Vališka, D. Braithwaite, G. Lapertot, M. Nardone, A. Zitouni, S. Mishra, I. Sheikin, G. Seyfarth, J.-P. Brison, D. Aoki, and J. Flouquet, Field-reentrant superconductivity close to a metamagnetic transition in the heavy-fermion superconductor UTe_2, J. Phys. Soc. Jpn. **88**, 063707 (2019).

[10] S. Ran, I.-L. Liu, Y. S. Eo, D. J. Campbell, P. M. Neves, W. T. Fuhrman, S. R. Saha, C. Eckberg, H. Kim, D. Graf, F. Balakirev, J. Singleton, J. Paglione, and N. P. Butch, Extreme magnetic field-boosted superconductivity, Nat. Phys. **15**, 1250 (2019).

[11] K. Kinjo, H. Fujibayashi, S. Kitagawa, K. Ishida, Y. Tokunaga, H. Sakai, S. Kambe, A. Nakamura, Y. Shimizu, Y. Homma, D. X. Li, F. Honda, D. Aoki, K. Hiraki, M. Kimata, and T. Sasaki, Change of superconducting character in UTe_2 induced by magnetic field, Phys. Rev. B **107**, L060502 (2023).

[12] A. Miyake, Y. Shimizu, Y. J. Sato, D. Li, A. Nakamura, Y. Homma, F. Honda, J. Flouquet, M. Tokunaga, and D. Aoki, Metamagnetic transition in heavy fermion superconductor UTe_2, J. Phys. Soc. Jpn. **88**, 063706 (2019).

[13] A. Miyake, M. Gen, A. Ikeda, K. Miyake, Y. Shimizu, Y. J. Sato, D. Li, A. Nakamura, Y. Homma, F. Honda, J. Flouquet, M. Tokunaga, and D. Aoki, Magnetovolume effect on the first-order metamagnetic transition in UTe_2, J. Phys. Soc. Jpn. **91**, 063703 (2022).

[14] W. Knafo, M. Vališka, D. Braithwaite, G. Lapertot, G. Knebel, A. Pourret, J.-P. Brison, J. Flouquet, and D. Aoki, Magnetic-field-induced phenomena in the paramagnetic superconductor UTe_2, J. Phys. Soc. Jpn. **88**, 063705 (2019).

[15] S. Imajo, Y. Kohama, A. Miyake, C. Dong, M. Tokunaga, J. Flouquet, K. Kindo, and D. Aoki, Thermodynamic investigation of metamagnetism in pulsed high magnetic fields on heavy fermion superconductor UTe_2, J. Phys. Soc. Jpn. **88**, 083705 (2019).

[16] A. Miyake, Y. Shimizu, Y. J. Sato, D. Li, A. Nakamura, Y. Homma, F. Honda, J. Flouquet, M. Tokunaga, and D. Aoki, Enhancement and discontinuity of effective mass through the first-order metamagnetic transition in UTe_2, J. Phys. Soc. Jpn. **90**, 103702 (2021).

[17] T. Thebault, M. Vališka, G. Lapertot, A. Pourret, D. Aoki, G. Knebel, D. Braithwaite, and W. Knafo, Anisotropic signatures of electronic correlations in the electrical resistivity of UTe_2, Phys. Rev. B **106**, 144406 (2022).

[18] Y. Tokunaga, H. Sakai, S. Kambe, P. Opletal, Y. Tokiwa, Y. Haga, S. Kitagawa, K. Ishida, D. Aoki, G. Knebel, G. Lapertot, S. Krämer, and M. Horvatić, Longitudinal spin fluctuations driving field-reinforced superconductivity in UTe_2, Phys. Rev. Lett. **131**, 226503 (2023).

[19] Q. Niu, G. Knebel, D. Braithwaite, D. Aoki, G. Lapertot, M. Vališka, G. Seyfarth, W. Knafo, T. Helm, J.-P. Brison, J. Flouquet, and A. Pourret, Evidence of Fermi surface reconstruction at the metamagnetic transition of the strongly correlated superconductor UTe_2, Phys. Rev. Res. **2**, 033179 (2020).

[20] T. Helm, M. Kimata, K. Sudo, A. Miyata, J. Stirnat, T. Förster, J. Hornung, M. König, I. Sheikin, A. Pourret, G. Lapertot, D. Aoki, G. Knebel, J. Wosnitza, and J.-P. Brison, Field-induced compensation of magnetic exchange as the possible origin of reentrant superconductivity in UTe_2, Nat. Commun. **15**, 37 (2024).

[21] L. Jiao, S. Howard, S. Ran, Z. Wang, J. O. Rodriguez, M. Sigrist, Z. Wang, N. P. Butch, and V. Madhavan, Chiral superconductivity in heavy-fermion metal UTe_2, Nature (London) **579**, 523 (2020).

[22] I. M. Hayes, D. S. Wei, T. Metz, J. Zhang, Y. S. Eo, S. Ran, S. R. Saha, J. Collini, N. P. Butch, D. F. Agterberg, A. Kapitulnik, and J. Paglione, Multicomponent superconducting order parameter in UTe_2, Science **373**, 797 (2021).

[23] N. Azari, M. Yakovlev, N. Rye, S. R. Dunsiger, S. Sundar, M. M. Bordelon, S. M. Thomas, J. D. Thompson, P. F. S. Rosa, and J. E. Sonier, Absence of spontaneous magnetic fields due to time-reversal symmetry breaking in bulk superconducting UTe_2, Phys. Rev. Lett. **131**, 226504 (2023).

[24] M. O. Ajeesh, M. Bordelon, C. Girod, S. Mishra, F. Ronning, E. D. Bauer, B. Maiorov, J. D. Thompson, P. F. S. Rosa, and S. M. Thomas, The fate of time-reversal symmetry breaking in UTe_2, Phys. Rev. X **13**, 041019 (2023)

[25] D. Braithwaite, M. Vališka, G. Knebel, G. Lapertot, J. P. Brison, A. Pourret, M. E. Zhitomirsky, J. Flouquet, F. Honda, and D. Aoki, Multiple superconducting phases in a nearly ferromagnetic system, Commun. Phys. **2**, 147 (2019).

[26] S. M. Thomas, C. Stevens, F. B. Santos, S. S. Fender, E. D. Bauer, F. Ronning, J. D. Thompson, A. Huxley, and P. F. S. Rosa, Spatially inhomogeneous superconductivity in UTe_2, Phys. Rev. B **104**, 224501 (2021).

[27] W.-C. Lin, D. J. Campbell, S. Ran, I.-L. Liu, H. Kim, A. H. Nevidomskyy, D. Graf, N. P. Butch, and J. Paglione, Tuning magnetic confinement of spin-triplet superconductivity, npj Quantum Mater. **5**, 68 (2020).

[28] D. Aoki, F. Honda, G. Knebel, D. Braithwaite, A. Nakamura, D. X. Li, Y. Homma, Y. Shimizu, Y. J. Sato, J. P. Brison, and J. Flouquet, Multiple superconducting phases and unusual enhancement of the upper critical field in UTe_2, J. Phys. Soc. Jpn. **89**, 053705 (2020).

[29] S. Ran, H. Kim, I.-Lin Liu, S. R. Saha, I. Hayes, T. Metz, Y. S. Eo, J. Paglione, and N. P. Butch, Enhancement and reentrance of spin triplet superconductivity in UTe_2 under pressure, Phys. Rev. B **101**, 140503(R) (2020).

[30] W. Knafo, T. Thebault, P. Manuel, D. D. Khalyavin, F. Orlandi, E. Ressouche, K. Beauvois, G. Lapertot, K. Kaneko, D. Aoki, D. Braithwaite, G. Knebel, and S. Raymond, Incommensurate antiferromagnetism in UTe_2 under pressure, arXiv:2311.05455.

[31] D. Li, A. Nakamura, F. Honda, Y. J. Sato, Y. Homma, Y. Shimizu, J. Ishizuka, Y. Yanase, G. Knebel, J. Flouquet, and D. Aoki, Magnetic properties under pressure in novel spin-triplet superconductor UTe_2, J. Phys. Soc. Jpn. **90**, 073703 (2021).

[32] S. M. Thomas, F. B. Santos, M. H. Christensen, T. Asaba, F. Ronning, J. D. Thompson, E. D. Bauer, R. M. Fernandes, G. Fabbris, and P. F. S. Rosa, Evidence for a pressure-induced antiferromagnetic quantum critical point in intermediate-valence UTe_2, Sci. Adv. **6**, eabc8709 (2020).

[33] M. Vališka, W. Knafo, G. Knebel, G. Lapertot, D. Aoki, and D. Braithwaite, Magnetic reshuffling and feedback on superconductivity in UTe_2 under pressure, Phys. Rev. B **104**, 214507 (2021).

[34] K. Kinjo, H. Fujibayashi, G. Nakamine, S. Kitagawa, K. Ishida, Y. Tokunaga, H. Sakai, S. Kambe, A. Nakamura, Y. Shimizu, Y. Homma, D. Li, F. Honda, and D. Aoki, Drastic change in magnetic anisotropy of UTe_2 under pressure revealed by ^{125}Te-NMR, Phys. Rev. B **105**, L140502 (2022).

[35] D. Aoki, M. Kimata, Y. J. Sato, G. Knebel, F. Honda, A. Nakamura, D. Li, Y. Homma, Y. Shimizu, W. Knafo, D. Braithwaite, M. Vališka, A. Pourret, J.-P. Brison, and J. Flouquet, Field-induced superconductivity near the superconducting critical pressure in UTe_2, J. Phys. Soc. Jpn. **90**, 074705 (2021).

[36] Y. Xu, Y. Sheng, and Y.-F. Yang, Quasi-two-dimensional Fermi surfaces and unitary spin-triplet pairing in the heavy fermion superconductor UTe_2, Phys. Rev. Lett. **123**, 217002 (2019).

[37] J. Ishizuka, S. Sumita, A. Daido, and Y. Yanase, Insulator-metal transition and topological superconductivity in UTe_2 from a first-principles calculation, Phys. Rev. Lett. **123**, 217001 (2019).

[38] S.-i. Fujimori, I. Kawasaki, Y. Takeda, H. Yamagami, A. Nakamura, Y. Homma, and D. Aoki, Electronic structure of UTe_2 studied by photoelectron spectroscopy, J. Phys. Soc. Jpn. **88**, 103701 (2019).

[39] L. Miao, S. Liu, Y. Xu, E. C. Kotta, C.-J. Kang, S. Ran, J. Paglione, G. Kotliar, N. P. Butch, J. D. Denlinger, and L. A. Wray, Low energy band structure and symmetries of UTe_2 from angle-resolved photoemission spectroscopy, Phys. Rev. Lett. **124**, 076401 (2020).

[40] T. Shishidou, H. G. Suh, P. M. R. Brydon, M. Weinert, and D. F. Agterberg, Topological band and superconductivity in UTe_2, Phys. Rev. B **103**, 104504 (2021).

[41] H. C. Choi, S. H. Lee, and B.-J. Yang, Correlated normal state fermiology and topological superconductivity in UTe_2, arXiv:2206.04876.

[42] D. Aoki, H. Sakai, P. Opletal, Y. Tokiwa, J. Ishizuka, Y. Yanase, H. Harima, A. Nakamura, D. Li, Y. Homma, Y. Shimizu, G. Knebel, J. Flouquet, and Y. Haga, First observation of the de Haas–van Alphen effect and Fermi surfaces in the unconventional superconductor UTe_2, J. Phys. Soc. Jpn. **91**, 083704 (2022).

[43] A. G. Eaton, T. I. Weinberger, N. J. M. Popiel, Z. Wu, A. J. Hickey, A. Cabala, J. Pospíšil, J. Prokleška, T. Haidamak, G. Bastien, P. Opletal, H. Sakai, Y. Haga, R. Nowell, S. M. Benjamin, V. Sechovský, G. G. Lonzarich, F. M. Grosche, and M. Vališka, Quasi-2D Fermi surface in the anomalous superconductor UTe_2, Nat. Commun. **15**, 223 (2024).

[44] C. Broyles, Z. Rehfuss, H. Siddiquee, J. A. Zhu, K. Zheng, M. Nikolo, D. Graf, J. Singleton, and S. Ran, Revealing a 3D Fermi surface pocket and electron-hole tunneling in UTe_2 with quantum oscillations, Phys. Rev. Lett. **131**, 036501 (2023).

[45] D. Aoki, I. Sheikin, A. McCollam, J. Ishizuka, Y. Yanase, G. Lapertot, J. Flouquet, and G. Knebel, de Haas–van Alphen oscillations for the field along c-axis in UTe_2, J. Phys. Soc. Jpn. **92**, 065002 (2023).

[46] Y. S. Eo, S. Liu, S. R. Saha, H. Kim, S. Ran, J. A. Horn, H. Hodovanets, J. Collini, T. Metz, W. T. Fuhrman, A. H. Nevidomskyy, J. D. Denlinger, N. P. Butch, M. S. Fuhrer, L. A. Wray, and J. Paglione, c-axis transport in UTe_2: Evidence of three-dimensional conductivity component, Phys. Rev. B **106**, L060505 (2022).

[47] C. Girod, C. R. Stevens, A. Huxley, E. D. Bauer, F. B. Santos, J. D. Thompson, R. M. Fernandes, J.-X. Zhu, F. Ronning, P. F. S. Rosa, and S. M. Thomas, Thermodynamic and electrical transport properties of UTe_2 under uniaxial stress, Phys. Rev. B **106**, L121101 (2022).

[48] H. Kim, I.-L. Liu, W.-C. Lin, Y. S. Eo, S. Ran, N. P. Butch, and J. Paglione, Tuning a magnetic energy scale with pressure in UTe_2, arXiv:2307.00180.

[49] K. Willa, F. Hardy, D. Aoki, D. Li, P. Wiecki, G. Lapertot, and C. Meingast, Thermodynamic signatures of short-range magnetic correlations in UTe_2, Phys. Rev. B **104**, 205107 (2021).

[50] Q. Niu, G. Knebel, D. Braithwaite, D. Aoki, G. Lapertot, G. Seyfarth, J.-P. Brison, J. Flouquet, and A. Pourret, Fermi-surface instability in the heavy-fermion superconductor UTe_2, Phys. Rev. Lett. **124**, 086601 (2020).

[51] Y. Tokunaga, H. Sakai, S. Kambe, Y. Haga, Y. Tokiwa, P. Opletal, H. Fujibayashi, K. Kinjo, S. Kitagawa, K. Ishida, A. Nakamura, Y. Shimizu, Y. Homma, D. Li, F. Honda, and D. Aoki, Slow electronic dynamics in the paramagnetic state of UTe_2, J. Phys. Soc. Jpn. **91**, 023707 (2022).

[52] N. P. Butch, S. Ran, S. R. Saha, P. M. Neves, M. P. Zic, J. Paglione, S. Gladchenko, Q. Ye, and J. A. Rodriguez-Rivera, Symmetry of magnetic correlations in spin-triplet superconductor UTe_2, npj Quantum Mater. **7**, 39 (2022).

[53] C. Duan, K. Sasmal, M. B. Maple, A. Podlesnyak, J.-X. Zhu, Q. Si, and P. Dai, Incommensurate spin fluctuations in the spin-triplet superconductor candidate UTe_2, Phys. Rev. Lett. **125**, 237003 (2020).

[54] W. Knafo, G. Knebel, P. Steffens, K. Kaneko, A. Rosuel, J.-P. Brison, J. Flouquet, D. Aoki, G. Lapertot, and S. Raymond, Low-dimensional antiferromagnetic fluctuations in the heavy-fermion paramagnetic ladder compound UTe_2, Phys. Rev. B **104**, L100409 (2021).

[55] C. Duan, R. E. Baumbach, A. Podlesnyak, Y. Deng, C. Moir, A. J. Breindel, M. B. Maple, E. M. Nica, Q. Si, and P. Dai, Resonance from antiferromagnetic spin fluctuations for superconductivity in UTe_2, Nature (London) **600**, 636 (2021).

[56] S. Raymond, W. Knafo, G. Knebel, K. Kaneko, J.-P. Brison, J. Flouquet, D. Aoki, and G. Lapertot, Feedback of supercon-

ductivity on the magnetic excitation spectrum of UTe_2, J. Phys. Soc. Jpn. **90**, 113706 (2021).

[57] D. Aoki, A. Nakamura, F. Honda, D. Li, Y. Homma, Y. Shimizu, Y. J. Sato, G. Knebel, J.-p. Brison, A. Pourret, D. Braithwaite, G. Lapertot, Q. Niu, M. Vališka, H. Harima, and J. Flouquet, Spin-triplet superconductivity in UTe_2 and ferromagnetic superconductors, JPS Conf. Proc. **30**, 011065 (2020).

[58] H. Sakai, P. Opletal, Y. Tokiwa, E. Yamamoto, Y. Tokunaga, S. Kambe, and Y. Haga, Single crystal growth of superconducting UTe_2 by molten salt flux method, Phys. Rev. Mater. **6**, 073401 (2022).

[59] R. Küchler, T. Bauer, M. Brando, and F. Steglich, A compact and miniaturized high resolution capacitance dilatometer for measuring thermal expansion and magnetostriction, Rev. Sci. Instrum. **83**, 095102 (2012).

[60] H. Sakai, Y. Tokiwa, P. Opletal, M. Kimata, S. Awaji, T. Sasaki, D. Aoki, S. Kambe, Y. Tokunaga, and Y. Haga, Field induced multiple superconducting phases in UTe_2 along hard magnetic axis, Phys. Rev. Lett. **130**, 196002 (2023).

[61] Only close to the critical metamagnetic field, the temperature dependence seems to be stronger than T^2, however, in the analysis we forced the fit to be T^2, neglecting the initial curvature in this plot very close to T_{SC}.

[62] A. C. Jacko, J. O. Fjærestad, and B. J. Powell, A unified explanation of the Kadowaki–Woods ratio in strongly correlated metals, Nat. Phys. **5**, 422 (2009).

[63] S. Khmelevskyi, L. V. Pourovskii, and E. A. Tereshina-Chitrova, Structure of the normal state and origin of the Schottky anomaly in the correlated heavy-fermion superconductor UTe_2, Phys. Rev. B **107**, 214501 (2023).

[64] W. Knafo, M. Nardone, M. Valiska, A. Zitouni, G. Lapertot, D. Aoki, G. Knebel, and D. Braithwaite, Comparison of two superconducting phases induced by a magnetic field in UTe_2, Commun Phys **4**, 40 (2020).

[65] M. Boukahil, A. Pourret, G. Knebel, D. Aoki, Y. Ōnuki, and J. Flouquet, Lifshitz transition and metamagnetism: Thermoelectric studies of $CeRu_2Si_2$, Phys. Rev. B **90**, 075127 (2014).

[66] T. D. Matsuda, H. Sugawara, Y. Aoki, H. Sato, A. V. Andreev, Y. Shiokawa, V. Sechovsky, and L. Havela, Transport properties of the anisotropic itinerant-electron metamagnet UCoAl, Phys. Rev. B **62**, 13852 (2000).

[67] A. de Visser, K. Bakker, L. Tai, A. Menovsky, S. Mentink, G. Nieuwenhuys, and J. Mydosh, High-field magnetoresistance of heavy-fermion UPd_2Al_3, Physica B (Amsterdam) **186-188**, 291 (1993).

[68] H. Aoki, N. Kimura, and T. Terashima, Fermi surface properties, metamagnetic transition and quantum phase transition of $CeRu_2Si_2$ and its alloys probed by the dHvA effect, J. Phys. Soc. Jpn. **83**, 072001 (2014).

[69] A. Palacio-Morales, A. Pourret, G. Knebel, T. Combier, D. Aoki, H. Harima, and J. Flouquet, Metamagnetic transition in UCoAl probed by thermoelectric measurements, Phys. Rev. Lett. **110**, 116404 (2013).

[70] T. Terashima, C. Haworth, M. Takashita, H. Aoki, N. Sato, and T. Komatsubara, Heavy fermions survive the metamagnetic transition in UPd_2Al_3, Phys. Rev. B **55**, R13369 (1997).

[71] Determining the intrinsic width of the superconducting transition from the resistivity is not possible, as a single superconducting path through the sample can yield $\rho = 0$, whereas specific heat reveals the transition in the whole sample volume.

[72] Z. Wu, T. I. Weinberger, J. Chen, A. Cabala, D. V. Chichinadze, D. Shaffer, J. Pospisil, J. Prokleska, T. Haidamak, G. Bastien, V. Sechovsky, A. J. Hickey, M. J. Mancera-Ugarte, S. Benjamin, D. E. Graf, Y. Skourski, G. G. Lonzarich, M. Valiska, F. M. Grosche, and A. G. Eaton, Enhanced triplet superconductivity in next generation ultraclean UTe_2, arXiv:2305.19033.

[73] Y. Tokiwa, H. Sakai, S. Kambe, P. Opletal, E. Yamamoto, M. Kimata, S. Awaji, T. Sasaki, Y. Yanase, Y. Haga, and Y. Tokunaga, Anomalous vortex dynamics in the spin-triplet superconductor UTe_2, Phys. Rev. B **108**, 144502 (2023).

[74] T. Park, F. Ronning, H. Q. Yuan, M. B. Salamon, R. Movshovich, J. L. Sarrao, and J. D. Thompson, Hidden magnetism and quantum criticality in the heavy fermion superconductor $CeRhIn_5$, Nature (London) **440**, 65 (2006).

[75] G. Knebel, D. Aoki, D. Braithwaite, B. Salce, and J. Flouquet, Coexistence of antiferromagnetism and superconductivity in $CeRhIn_5$ under high pressure and magnetic field, Phys. Rev. B **74**, 020501(R) (2006).

[76] S. Ran, S. R. Saha, I.-L. Liu, D. Graf, J. Paglione, and N. P. Butch, Expansion of the high field-boosted superconductivity in UTe_2 under pressure, npj Quantum Mater. **6**, 75 (2021).

[77] D. V. Ambika, Q.-P. Ding, K. Rana, C. E. Frank, E. L. Green, S. Ran, N. P. Butch, and Y. Furukawa, Possible coexistence of antiferromagnetic and ferromagnetic spin fluctuations in the spin-triplet superconductor UTe_2 revealed by ^{125}Te NMR under pressure, Phys. Rev. B **105**, L220403 (2022).

[78] K. Kinjo, H. Fujibayashi, H. Matsumura, F. Hori, S. Kitagawa, K. Ishida, Y. Tokunaga, H. Sakai, S. Kambe, A. Nakamura, Y. Shimizu, Y. Homma, D. Li, F. Honda, and D. Aoki, Superconducting spin reorientation in spin-triplet multiple superconducting phases of UTe_2, Sci. Adv. **9**, eadg2736 (2023).

[79] J. Ishizuka and Y. Yanase, Periodic Anderson model for magnetism and superconductivity in UTe_2, Phys. Rev. B **103**, 094504 (2021).

[80] Y. Tokunaga, H. Sakai, S. Kambe, T. Hattori, N. Higa, G. Nakamine, S. Kitagawa, K. Ishida, A. Nakamura, Y. Shimizu, Y. Homma, D. Li, F. Honda, and D. Aoki, ^{125}Te-NMR study on a single crystal of heavy fermion superconductor UTe_2, J. Phys. Soc. Jpn. **88**, 073701 (2019).

[81] F. Wilhelm, J.-P. Sanchez, D. Braithwaite, G. Knebel, G. Lapertot, and A. Rogalev, Investigating the electronic states of UTe_2 using x-ray spectroscopy, Commun. Phys. **6**, 96 (2023).